2020-01-01

A Probabilistic Creep Constitutive Model for Creep Deformation, Damage, and Rupture

Md Abir Hossain
University of Texas at El Paso

A PROBABILISTIC CREEP CONSTITUTIVE MODEL FOR CREEP DEFORMATION, DAMAGE, AND RUPTURE

MD ABIR HOSSAIN

Master's Program in Mechanical Engineering

APPROVED:

Calvin M. Stewart, Ph.D., Chair

Jack F. Chessa, Ph.D.

Cesar Carrasco, Ph.D.

Stephen L. Crites, Jr., Ph.D.
Dean of the Graduate School

Dedication

Dedicated to my parents.

Md Rafiqul Alam Mojumdar and Kamrun Nahar

“Thank you for making it a family,

For giving it meaning,

For filling it with Love”

A PROBABILISTIC CREEP CONSTITUTIVE MODEL FOR CREEP DEFORMATION, DAMAGE, AND RUPTURE

by

MD ABIR HOSSAIN, B.Sc.

THESIS

Presented to the Faculty of the Graduate School of

The University of Texas at El Paso

in Partial Fulfillment

of the Requirements

for the Degree of

MASTER OF SCIENCE

Department of Mechanical Engineering

THE UNIVERSITY OF TEXAS AT EL PASO

August 2020

Acknowledgements

I would like to express the deepest appreciation to my committee chair and research advisor Dr. Calvin M. Stewart, who has the attitude and the substance of a genius; he continually conveyed a spirit of adventure in regards to research and investigation, and an excitement in regards to analysis and experiment. Without his guidance and persistent help this thesis would not have been come to fruition. It was a great privilege and honor to study and work under his guidance.

I would like to thank my committee members, Dr. Jack F. Chessa and Dr. Cesar Carrasco who supported me with their insights and technical nous of the realm of uncertainty quantification and probabilistic modeling.

I am extremely grateful to my parents for their love, prayers, care, and sacrifices for educating me and preparing me for my future. In addition, a big shout out to all my colleagues, group members, and friends who have provided me with technical, emotional, and spiritual support in my pursuit to graduate studies and beyond.

Abstract

The structural analysis of Industrial Gas Turbine (IGT), Aeroengine, Gen IV nuclear components under in-service conditions at various stress and temperature are susceptible to time-dependent creep deformation and creep induced failure. Such failure phenomena are exacerbated by the randomness in material properties, oscillating loading conditions, and other sources of uncertainty. The demand for physically based probabilistic creep modeling is highly sought by alloy designers. The objective of this study is to develop and validate a probabilistic creep-damage model incorporating multi-sources of uncertainty to replace the traditional deterministic and empirical decision-based modeling. In this study, the deterministic Sine-hyperbolic (Sinh) creep-damage model is carefully tuned into a probabilistic model. The creep test data of alloy 304 stainless steel with replicates over a range of stress and temperature are gathered from the literature. First, the Sinh model is calibrated deterministically to determine the test-specific material constants and their associated statistical variability. A probabilistic framework is developed where the hypothesized sources of uncertainty: test conditions (stress and temperature), pre-existing damage, and material properties are introduced. The sources of uncertainties are carefully tuned based on the ASTM standards, statistical goodness-of-fit test, and the nature of deterministically calibrated constants. The probabilistic distribution function (pdfs) of each sources of uncertainty are determined in sequence to encapsulate the full experimental uncertainty. Single source probabilistic predictions are performed to determine the influence of each source of uncertainty on the creep deformation, damage, and rupture predictions. Full interaction probabilistic predictions are performed to demonstrate the interference effect of all the sources of uncertainty on the prediction of creep deformation, ductility, and rupture. The Sinh model constitutive equations are implemented into a USERCREEP.F, user material subroutine of the

ANSYS finite element software. For verification and validation (V&V), a finite element simulation in ANSYS Mechanical APDL (ANSYS Parametric Design Language) is conducted on 1-D and 2-D element model. Furthermore, the probabilistic model is applied to an expanded database of engineering alloys to validate the probabilistic prediction. Future work will focus on developing a multi-stage Sinh, stochasticity, time-dependent pdfs for improved uncertainty quantification.

Keywords: Creep; Life prediction; Monte Carlo method; Probabilistic; Reliability; Uncertainty.

Table of Contents

List of Tables

List of Figures

Chapter 1: Introduction

1.1 MOTIVATION

Drives to increase the efficiency of Advance Ultrasupercritical (A-USC) and Fossil Energy (FE) power plants lead to designs with steam pressures up to 4000 psi and temperatures ranging $0.3T_m < T < 0.5T_m$, where T_m is the melting temperature of the specific material. The complexity in which these power plants operate pushes the limits of material science and the properties of materials [1]. The power plant operation, especially for the hot gas path in industrial gas turbines (IGTs) illustrated in Figure 1.1 [2]. The complex components exposed to high loadings and temperature for entirety of service life are susceptible to creep and creep induced failures. The catastrophic failure, as illustrated in the turbine blade of Figure 1.2, caused by creep and combined damage factors [3]. Creep is a stress, temperature, and time dependent phenomenon that exhibits considerable scatter. When the results of many creep tests are aggregated, the minimum-creep-strain-rate (MCSR), stress-rupture (SR), and creep deformation curves exhibit substantial scattering. At normal operating conditions (low stress – high temperature), the SR data can scatter spanning logarithmic decades as shown in Figure 1.3 for Gr. 91 steel [4]. The accurate service life is difficult to estimate without extensive testing program, reliability analysis, inflated safety factors, and compromised design decision. The origin of the uncertainty stems from various sources; notably, test condition, service conditions, metallurgical inhomogeneities (due to thermomechanical processing, prior service, surface, and subsurface defects), geometric parameters, and test procedure error [5-8]. These random factors cannot be eliminated entirely from the experimentation, pre-processing, service condition, and modeling approaches and must be characterized adequately. The significance of uncertainty quantification is compounded when the high reliability and durability is demanded. The design process become intensive and weary

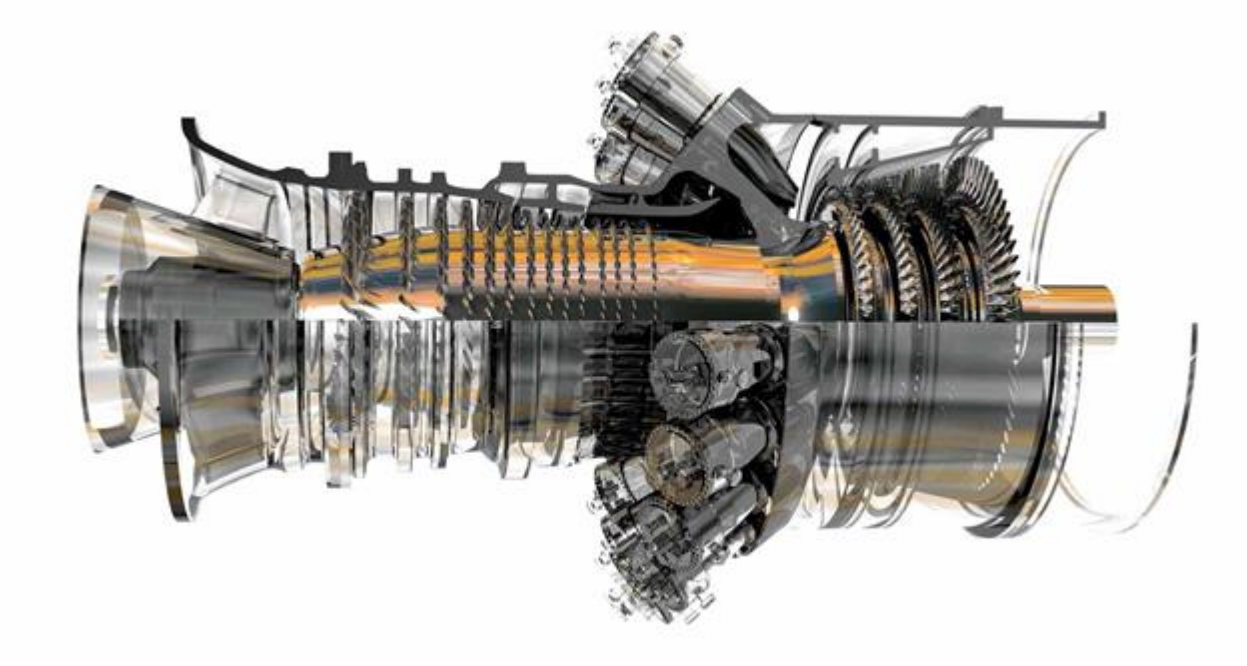

Figure 1.1 : GE H-Class 9HA.01/.02 Gas Turbine (50 Hz) (9HA.01 at 446 MW and the 9HA.02 at 571 MW) [2]

Figure 1.2 : Industrial gas turbine creep failure (Berkeley Research Company, Berkeley, California) [3]

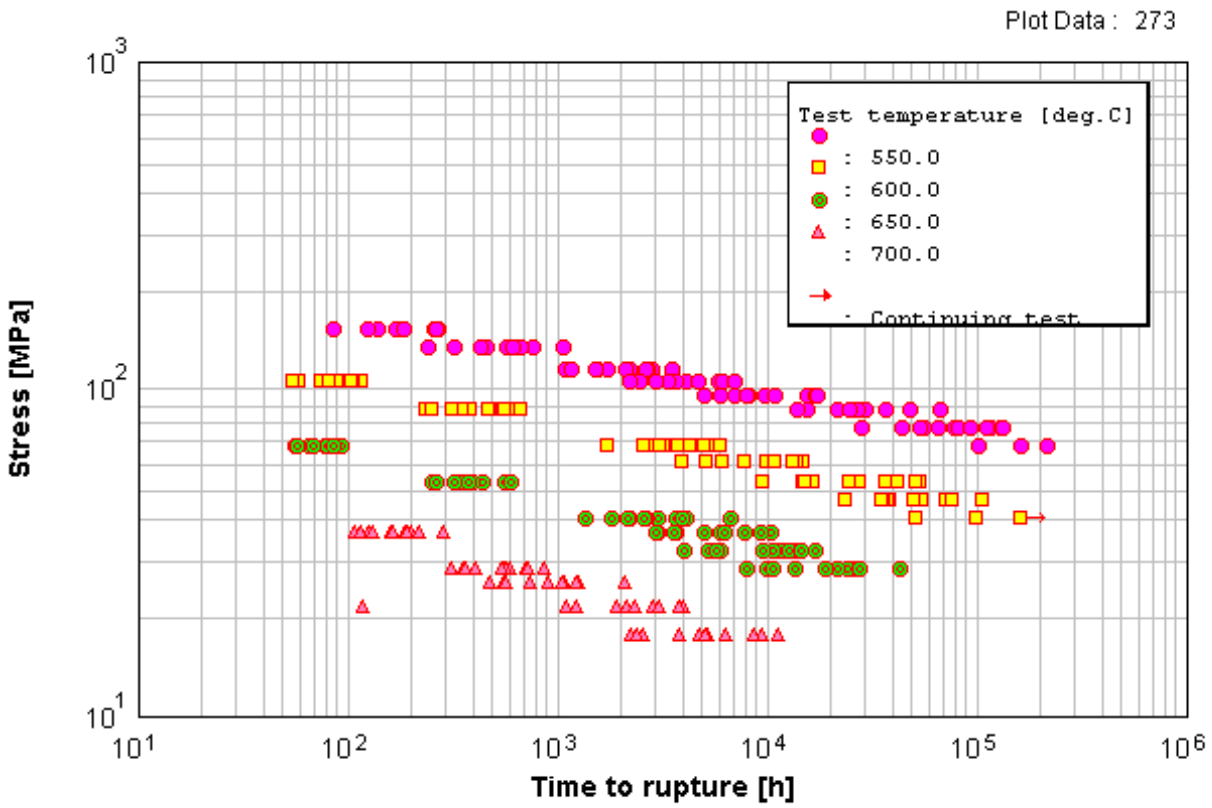

Figure 1.3 : Stress-rupture data of Gr. 91 steel gathered from NIMS database [4].

when there is limited to no experimental observation. In such instances, traditional deterministic and empirical decision-based modeling do not generate optimal solutions. There is a demand for rapid uncertainty quantification, reliability, and durability for reduced risk service life. Furthermore, new candidate alloys and superalloys design for complex components become challenging due to time and cost constraints. To address these concerns, the uncertainties in creep data should be integrated into probabilistic modeling approach to enable a more reliable prediction of creep deformation, damage evolution, and rupture in structures.

1.2 Research Objective

The objective of this study is to develop a probabilistic Sine-hyperbolic (Sinh) model to predict the uncertainty of creep deformation, damage, and rupture in alloys. To meet the research

goals, this thesis shall: (a) assess the Sinh model from a deterministic standpoint; (b) develop a probabilistic calibration approach; (c) perform a sensitivity analysis to determine the extent that each source of uncertainty contributes to creep resistance; (e) verify the deterministic model with finite element analysis; (d) perform the validation of full interaction probabilistic model against uncertain creep data.

1.3 ORGANIZATION

The organization of this study is as follows: Chapter 2 provides background information on creep, creep-damage, and uncertainties encountered in creep data. Existing probabilistic creep models and test programs to capture the experimental uncertainty are discussed in a non-exhaustive manner. Chapter 3 introduces and describes the material used in each study providing mechanical properties, nominal chemical composition, and scattering in creep data in replicated tests across multiple isostress-isotherm. Chapter 4 introduces the Sine-hyperbolic (Sinh) creep-damage model to be employed for deterministic and probabilistic predictions. The constitutive equation and calibration approach are discussed. Validation and verification (V&V) are performed and discussed in chapter 5 for both deterministic and probabilistic prediction. Finally, chapter 6 offers an overview of the results and concluding remarks as well as the future work.

Chapter 2: Background

2.1 Introduction

To develop a probabilistic creep model, a background study is needed to understand creep phenomenon. Creep is a phenomenological event that is divided in regimes. Thus far, many deterministic models are designed to understand MCSR, SR, and creep deformation behavior. A summary of the existing probabilistic models is discussed. To carefully tune a deterministic creep-damage model into a probabilistic one, an overview of recent probabilistic modeling approaches is needed to perceive the existing limitations. The probabilistic Sinh model is discussed later to give a stronger flow to the narrative.

2.2 Creep Phenomenon

Creep is the progressive time-dependent inelastic deformation under constant load and temperature. For many structural materials, creep is observed above a specified elevated temperature and loadings over an extended time of operation. Examples include structural components of power generation plants, chemical facilities, heat engines, and other high-temperature equipment. Creep and creep induced failure is accompanied by progressive deformation, relaxation and redistribution of stresses, local reduction of material strength, etc. The aim of creep modeling is to predict time-dependent changes of stress and strain up to the critical stage of creep rupture [9-10].

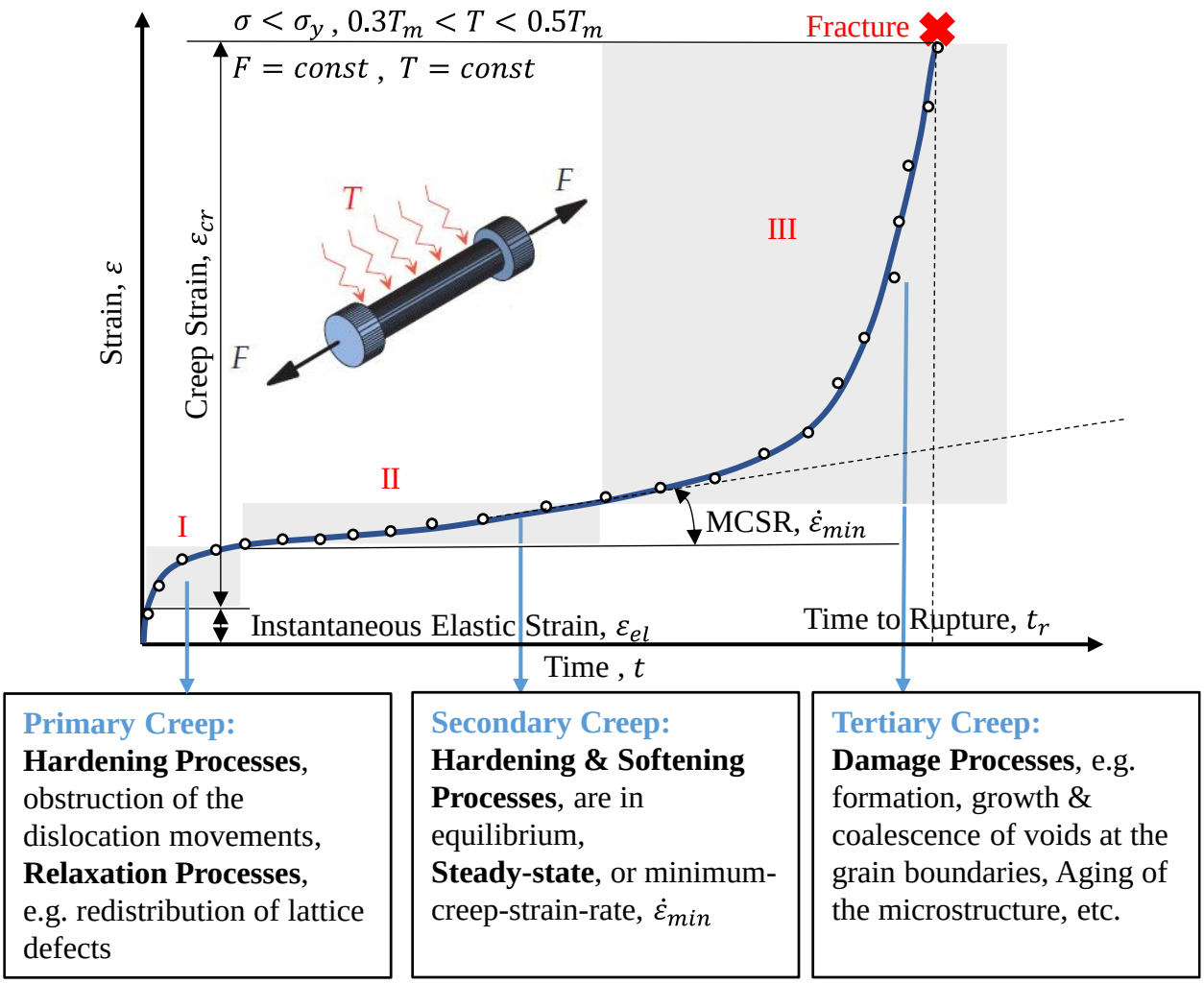

Figure 2.1 : Typical creep deformation curve under uniaxial loading F and temperature T (I – primary creep, II – secondary creep, III – tertiary creep) [10]

A number of creep material properties can be deduced from the uniaxial creep curve. The notable ones are the duration of the stages, the minimum-creep-strain-rate, $\dot{\varepsilon}_{\min}$, rupture time, t_r , and creep ductility, ε_{cr} . The shape of the creep curve is determined by several competing processes [11]. The reactions mainly include: strain hardening; softening processes such as recovery, recrystallization, strain softening, and precipitate overaging; Damaging processes such as cavitation and cracking, and specimen necking. Of these factors, strain hardening tends to decrease

the creep rate, $\dot{\varepsilon}_{cr}$, whereas the other factors tend to increase the creep rate, $\dot{\varepsilon}_{cr}$. The microstructural mechanism such as precipitate carbides prevents the grain boundary sliding. In tertiary regime, grain boundary sliding contributes to crack propagation and void nucleation and growth which ultimately leads to rupture in the specimen 11]. The interaction of these processes determine the shape of the creep curve [11-14].

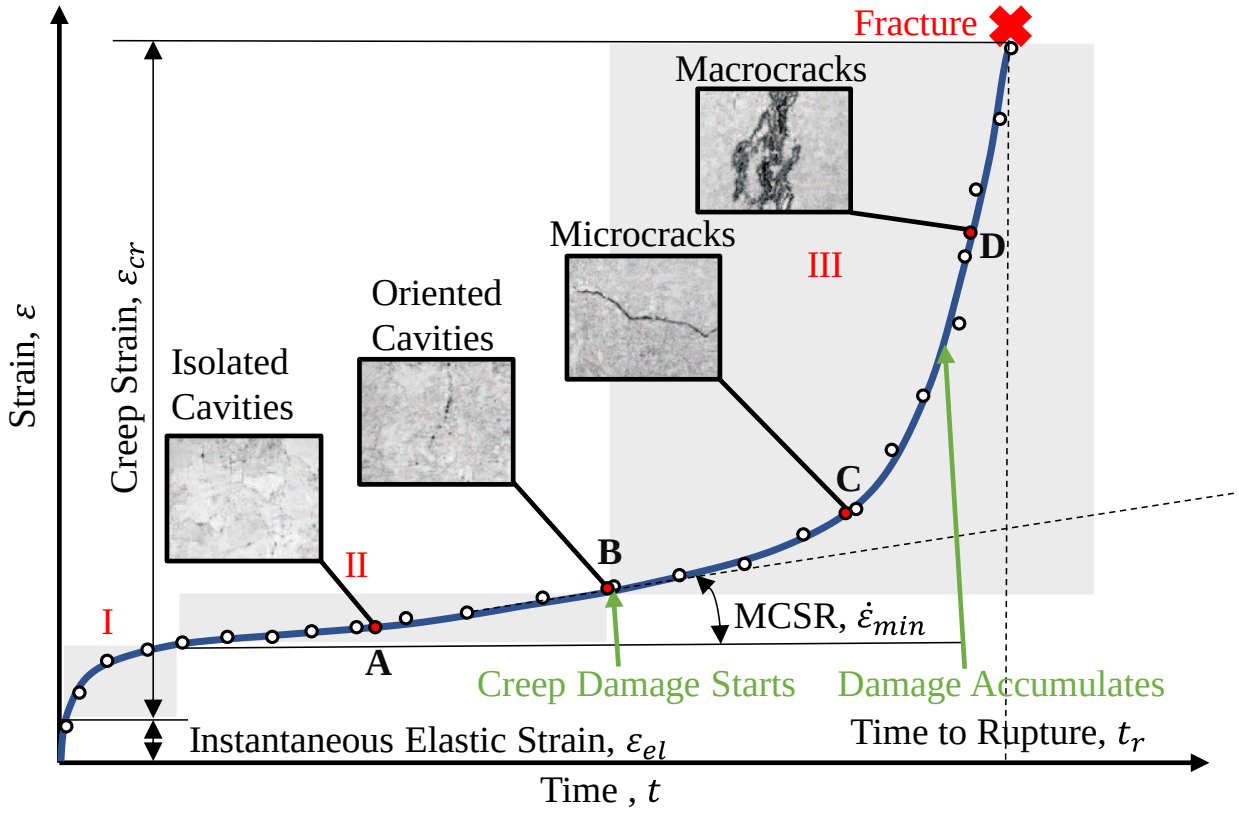

Figure 2.2 : Damage evolution caused by creep and corresponding service condition. Herein A – observation, B – observation, fixed inspection intervals, C – limited service until repair, D- immediate repair [15]

The creep behavior can be divided into three stages as shown in Figure 2.1. During primary creep, strain hardening causes the slope of the creep curve to decrease. Secondary creep is

explained in terms of balance between strain hardening and the softening processes resulting in nearly constant creep rate. During this stage, an equilibrium is achieved between the hardening and the damage in the material. The tertiary creep stage marks the onset of internal- or external-damage processes resulting in a decrease in the resistance to load or a significant increase in the net section stress. The softening process coupled with the balance achieved in secondary stage to achieve a rapidly increasing tertiary stage of creep. Note that some materials show no tertiary creep, others have a very short primary creep period.

Time-dependent creep deformation and damage processes are induced by the nucleation and the growth of microscopic cracks and cavities in metals and alloys. The creep induced damage evolution at various stages of a material life is shown in Figure 2.2. Damage accumulates in the form of internal cavities during creep. The damage first appears at the start of tertiary creep regime of the creep curve and grows at an increasing rate thereafter. The shape of tertiary creep regime of the creep curve reflects this : as the cavities grow, the cross-section of the specimen decreases, and at constant load the true stress, σ goes up. The creep rate, $\dot{\varepsilon}_{cr}$ goes up even faster than the true stress, σ does caused by creep damage. . To characterize the damage evolution and the increase of creep strain rate in tertiary creep regime, the continuum damage mechanics (CDM) has been established and demonstrated to be a powerful approach [16]. A lot of application of creep CDM are related to long-term predictions in power and chemical plants.

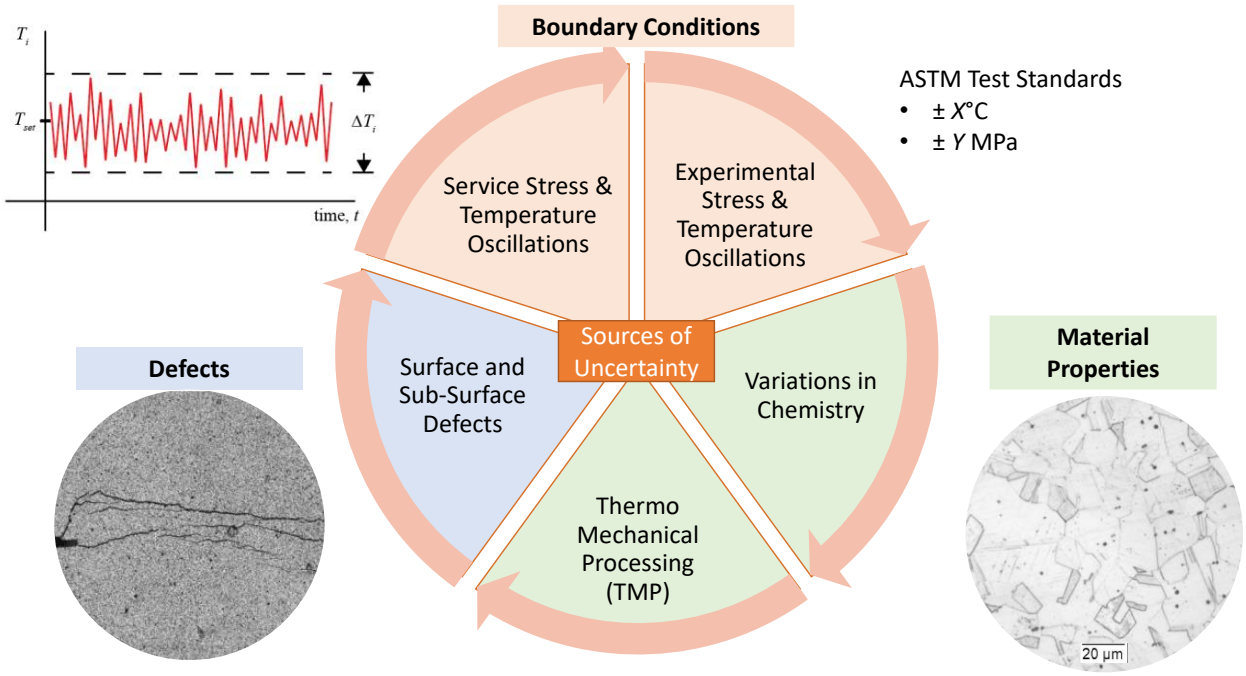

Figure 2.3 : Sources of uncertainty encountered in replicated creep test [5-8]

2.3 Uncertainty in Creep Data

By its very nature, creep deformation data takes a long time to accumulate and there is usually a remarkable amount of scattering in the data. For steels, within the nominal chemical composition, the creep rupture properties show considerable batch to batch scatter [17-24]. There are a number of sources of uncertainty that cause this scattering in the creep data. The most notable uncertainties are boundary condition uncertainty, material properties related uncertainty due to thermomechanical processing, surface and sub-surface defects and priori damage, model variations, geometric parameters, operator and machine error [5-8]. These varying sources of uncertainties are idealized in Figure 2.3. These and other uncertainties have justified the completion of replicant many long-term test programs for power plant steels in various product forms (e.g. tube, pipe, plate, and forgings). Studies of Rutmen et al. revealed the variation of creep rupture by an order of magnitude for two different high temperature alloy [17]. Creep rupture tests

on 316 stainless steel by Garofalo et al. revealed a rupture variation by a factor of 4.5 [18]. Penny et al. noticed the scattering of rupture on the order of 10 hours in the replicated creep rupture experiments [19]. Hayhurst directed his research towards explaining the effects of test variables on the scatter in creep data and revealed a small fluctuation of temperature ±3°C can lead to ±8% variation in creep rupture [20]. It was also reported that loading eccentricity of 1.5% can reduces the rupture life by up to 60%. Farris et al. showed experimental evidence for load eccentricity with creep rupture tests of copper-bicrystal exhibiting 60% life reduction due to 2-12% eccentric loading [21]. Kim et al. performed the short-term creep test on 304 Stainless Steel and found that Coefficient of variation (%CoV) of initial strain, minimum-creep-strain-rate, and creep ductility are two to three times higher than creep rupture [22]. Evans et al. statistically analyzed the creep rupture data of 0.25Cr-0.5Mo-0.25V and observed the scattering of failure time by a factor of 6-7 [23]. In a separate study by Booker et al. conducted on creep rupture properties of 2.25Cr-1Mo steel of 53 different heats of materials and concluded that average rupture time for single-heat vary over staggering range of 4000 to 100000 hours [24]. These wide ranges of scattering in creep deformation to rupture data spanning decades make the accurate lifetime estimation a cumbersome and crude procedure.

2.4 PROBABILISTIC CREEP MODELING

The probabilistic modeling begins with the selection of a random sampling method. The aim of random sampling method is to provide information on a given population by studying a subset of it [25-28]. Over the course of time, many probabilistic analysis methods are developed. Most of the methods are approximate in nature and strive to provide very efficient analysis. The selection of an appropriate method should be guided by several considerations, including required computational time, complexity of problems, and solution accuracy.

One of the most used random sampling methods for engineering and mathematical problem is Monte Carlo method. The Monte Carlo method uses the given sample to determine the probability of success and/or failure for the given constraints. Latin Hypercube Simulation (LHS) method is similar to Monte Carlo except that each input distribution is partitioned into equal probability intervals. For each random variable, one sample is taken from each probability interval. First- and Second- Order Reliability Method (FORM and SORM) provide the approximate estimates requiring much less model evaluation than Monte Carlo or Latin Hypercube sampling. These methods search for the most probable failure point (MPP) and then compute reliability based on an approximate to the constraint. The mean value (MV) method based on the derivatives of the performance function at the mean of the inputs. The advanced mean value (AMV) method constructs a first-order Taylor series approximation of the performance function at the mean of the inputs and uses this approximation to estimate the MPP. Response Surface Method (RSM) approximate a constraint using one of three experimental designs: Central Composite, Box Behnken, or Koshal (one at a time). Once the constraint is approximated with substantial reliability, Monte Carlo method is used to perform the probabilistic analysis. Gaussian Process Response Surface Response Method (RSM_GP) approximates the true limit state function by constructing a Gaussian Process response surface model. The Weiner process: often called Brownian Motion is employed to describe the complicated stochastic processes into the probabilistic analysis. The Bayesian Network is a probabilistic graphical model that represents a set of variables and their conditional dependencies via a directed acyclic graphs (DAG). The probabilistic methods are listed in Table 2.1.

Table 2.1 : The probabilistic methods in engineering, mathematical, and structural reliability analysis.

Acronym	Probabilistic Analysis Method
MONTE	Monte Carlo Method
LHS	Latin Hypercube Simulation
FORM	First Order Reliability Method
SORM	Second Order Reliability Method
MV	Mean Value Method
AMV	Advanced Mean Value Method
RSM	Response Surface Method
RSM_GP	Gaussian Process Response Surface Method
BM	Weiner Process/ Brownian Motion
BN	Bayesian Network

Creep constitutive models are often applied deterministically where scatter is not considered; rather, the best-line through the scattered data is the target of calibration. Creep models such as MPC-Omega, Theta-projection, Wilshire, and Sine-hyperbolic are employed in this fashion [29-32]. Deterministic models can be converted into probabilistic models by injecting uncertainty into their formulation.

Several “single-source” uncertainty models have been developed [33-38]. Appalanaidu developed a stochastic creep damage growth model where temperature uncertainty is modeled using white noise functions [33]. It was determined that the choice of noise function has a significant impact on the scatter in damage predictions. Harlow et al. proposed a probabilistic

Kachanov-Rabotnov CDM-based model where material property uncertainty is incorporating using probability distribution functions (pdfs) and exact relations from probability theory [34]. Hossain and Stewart developed a probabilistic CDM-based Sine-hyperbolic (Sinh) creep-damage model where material property uncertainty is added using normal distributions and Monte Carlo methods [35]. A similar framework was developed for Modified Wilshire Creep-damage model [36]. Appalanaidu et al. developed a stochastic finite element methodology for pipe where material properties are spatially uncertain (i.e., inhomogeneous) using 2-D non-Gaussian random fields [37]. Kim and colleagues employed four different probabilistic methods to add material property uncertainty into a creep-crack-growth-rate model (least square fitting method, mean value method, probabilistic distribution method, and Monte Carlo method) [38]. A comparison between the four methods showed that the Monte Carlo method is expected to achieve a more accurate and economically viable solution due to the inherent conservatism of the technique.

Other researchers have developed "multiple-source" of uncertainty models [21,40-42]. Penny et al proposed a stochastic Kachanov-Rabotnov (KR) CDM based model where load and material uncertainties are modeled using Monte Carlo methods [19]. Farris performed probabilistic stress-rupture simulations that included temperature, stress, and eccentricity uncertainty using Monte Carlo methods [21]. The three uncertainties matched the scatter observed in short-term data but did not capture the full experimental uncertainty in long-term data suggesting additional sources. Bhattacharya et al. proposed a CDM-based model that encompasses several categories of material property uncertainty, microstructural damage evolution properties, critical damage, and macroscopic material properties [40]. It was concluded that the source of uncertainty and the type of probability distribution function (normal, uniform, lognormal) applied have a large influence on the scatter observed in predictions. Vojdani et al. developed a stochastic creep-fatigue crack

propagation model that included geometric, material property, and operating condition uncertainty [5]. It was determined that a sensitivity analysis of the random parameters must be performed to elucidate the order of importance of the random variables. Kim and colleagues developed a service condition creep rupture interference (SCRI) model where both the cumulative uncertainty of stress-rupture test conditions and service conditions are considered in rupture predictions [41-42]. Monte Carlo simulations showed a rapid decrease in reliability of stress-rupture at higher fluctuation of service stress and temperature.

Chapter 3: Materials

Creep data for alloy 304 stainless steel (304 SS) is selected for this study. The 304 stainless steel is the most versatile and widely used stainless steel. Creep data across multiple isostress-isotherm is gathered form the literature [43]. The chemical composition of the alloy 304 SS is listed in Table 3.1.

Table 3.1 : Chemical composition (wt%) of 304 SS [43]

C	Si	Mn	P	S	Ni	Cr	Mo	Cu	N
0.02	0.40	1.83	0.029	0.009	8.13	18.22	0.24	2.06	0.102

The 304 stainless steel has high corrosion resistant, high ductility, excellent drawing, forming, and spinning properties. Upon cold work nonmagnetic 304 SS may become slightly magnetic. The room temperature tensile strength, yield strength, and elongation are 706 MPa, 490 MPa, and 18% respectively. The conventional creep test (CCT) were conducted at elevated temperature of 600, 650, and 700°C. The creep test specimens were of 6 mm gauge diameter and 30 mm gauge length, fabricated from 20 mm diameter bar and experiments were carried out according to ASTM E139 standard [44].

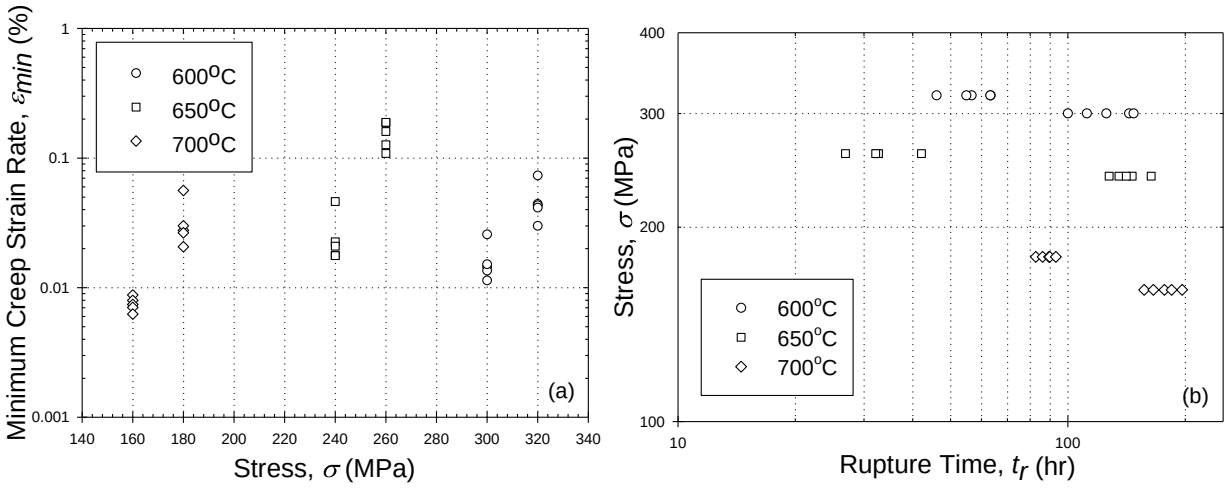

Figure 3.1 : Experimental scattering of (a) MCSR and (b) rupture time across multiple isostress.

A total of thirty creep curves were collected with tests conducted in quintuplicate (five repeats) at each stress range. The experimental MCSR and rupture time shows substantial scatter as shown in Figure 3.1. The test condition along with the statistical uncertainty of MCSR and rupture time are tabulated in Table 3.2. The coefficient of variation up to 48% and 16% are observed in the MCSR and rupture data respectively.

Table 3.2 : Statistical uncertainty of MCSR and rupture time of replicated creep test [43]

Temperature,	Stress,	MCSR, $\dot{\varepsilon}_{\min}$			Rupture, t_r		
T	σ	Max	Min	%COV	Max	Min	%COV
(°C)	(MPa)	(%·hr)	(%·hr)		(hr)	(hr)	
600	320	0.072	0.029	34.57	147.43	100.00	16.12
600	300	0.025	0.011	34.95	63.36	46.05	12.55
650	260	0.188	0.108	23.33	42.12	26.88	16.60

650	240	0.461	0.017	48.02	163.52	127.61	9.48
700	180	0.056	0.020	43.02	93.12	82.73	4.48
700	160	0.008	0.006	12.74	196.41	156.95	8.79

Chapter 4: Deterministic Creep-Damage Model

When subject to a high stress-temperature environment, 304 stainless steel (304 SS) is susceptible to creep and creep induced failure despite having high temperature strength, toughness, and resistance to degradation. The alloy 304 SS does not show an abrupt boundary between elastic and inelastic deformation rather shows a unified viscoplastic response [45]. Thus, it is susceptible to room temperature creep or relaxation depending on the applied boundary condition [45]. The creep response of the alloy 304 SS is critically important from a deterministic viewpoint.

Secondary creep-based classical life prediction models such as Larson-Miller, Manson-Hafred, or Monkman-Grant models can only predict the rupture life [46-48]. Tertiary creep regime can initiate quickly and unexpectedly under the high loadings and temperature where primary and secondary regimes are subordinate [49-50]. Often the primary creep regime is a short-lived phenomenon in creep deformation and can be neglected in gas turbine applications.

4.1 Sine-Hyperbolic (Sinh) Creep Damage Model

Recently, a novel multistage Sine-hyperbolic (Sinh) model has been developed by Stewart that can model secondary and tertiary creep stages [51]. The Sinh model has been applied to Waspaloy, 304 SS, alloy 18Cr-8Ni, alloy 18Cr-12Ni-Mo a systematic calibration approach exists for calibrating the conventional creep curves [29,34,52-53]. The Sinh model has been employed to deal with 3D notches using Hayhurst triaxial stress [52]. The Sinh model has been compared to Kachanov-Rabotnov (KR) model and found to exhibit less stress sensitivity, mesh-dependence, and better convergence [53]. The Sinh has been employed to deal with the disparate creep data where creep data is not always available in the quantity, quality, or type needed for modeling [54].

The temperature-dependent form of Sinh consists of a creep-strain-rate (CSR) and damage evolution equation as follows

$$\dot{\varepsilon}_{cr} = A\exp\left(\frac{-Q_c}{RT}\right)\sinh\left(\frac{\sigma}{\sigma_s}\right)\exp(\lambda\omega) \tag{4.1}$$

$$\dot{\omega} = \frac{[1-\exp(-\phi)]}{\phi} M \exp\left(\frac{-Q_c}{RT}\right)\sinh\left(\frac{\sigma}{\sigma_t}\right)^{\chi} \exp(\phi\omega) \tag{4.2}$$

where σ is stress, T is temperature in Kelvin, R is the universal gas constant, Q_c is the apparent activation energy, A and σ_s are the secondary creep constants, λ is the strain trajectory constant, M , σ_t , and χ are rupture constants, ϕ is the damage trajectory constant, and ω is damage an internal state variable that evolves from an initial damage, ω_0 to unity [53]. These equations can be simplified for isothermal conditions by setting $\exp\left(-Q_c/RT\right)=1$.

Assume that initial damage is zero, $\omega_0 = 0$. The secondary creep material constants, A and σ_s, can be calibrated using the "temperature-normalized" minimum-creep-strain-rate (MCSR)

$$\frac{\dot{\varepsilon}_{\min}}{\exp\left(\frac{-Q_c}{RT}\right)} = A\sinh\left(\frac{\sigma}{\sigma_s}\right) \tag{4.3}$$

where the $\dot{\varepsilon}_{\min}$ is the minimum-creep-strain-rate (MCSR) measured from creep data. The activation energy, Q_c is obtained by maximizing the log-log square of the Pearson product moment correlation coefficient of a regression line through MCSR or stress-rupture (SR) data.

The λ and ϕ constants exhibit stress and temperature dependence. The strain trajectory constants, λ is unitless and equal to

$$\lambda = \ln\left(\frac{\dot{\varepsilon}_{\text{final}}}{\dot{\varepsilon}_{\min}}\right) \tag{4.4}$$

where $\dot{\varepsilon}_{\text{final}}$ is the final-creep-strain-rate (FCSR) measured from creep data and $\lambda \geq 0$. The damage-trajectory constant ϕ is unitless and equal to

$$\phi = \ln\left(\frac{\dot{\omega}_{\text{final}}}{\dot{\omega}_{\min}}\right) \tag{4.5}$$

where the minimum-damage-rate, $\dot{\omega}_{\min}$ and final-damage-rate, $\dot{\omega}_{\text{final}}$ are not experimentally measured but can be analytical calculated and $\phi \geq 1$. Analytical damage, ω^* and damage rates, $\dot{\omega}^*$ data can be calculated from [Eq. (4.1)] as follows

$$\begin{aligned} \omega^* &= \frac{1}{\lambda}\ln\left(\frac{\dot{\varepsilon}_{cr}}{\dot{\varepsilon}_{\min}}\right) \\ \dot{\omega}^* &= \frac{\Delta\omega^*}{\Delta t} \end{aligned} \tag{4.6}$$

The creep strain trajectory constant, λ and damage trajectory constant, ϕ exhibit stress and temperature-dependence. The dependencies of λ and ϕ are modeled according to Eyring's equations

$$\lambda(\sigma, T) = \lambda_0 \exp\left(-\frac{V_\lambda^* \sigma}{k_b T}\right) \tag{4.7}$$
$$\lambda \geq 0$$

$$\phi(\sigma, T) = \phi_0 \exp\left(\frac{V_\phi^* \sigma}{k_b T}\right) \tag{4.8}$$
$$\phi \geq 1$$

where λ_0 and ϕ_0 are a unitless coefficients, V_λ^* and V_ϕ^* are the activation volume for λ and ϕ respectively, σ is stress , T is temperature, and k_b is the Boltzmann constant.

Integration of the damage evolution [Eq. (4.2)] furnishes damage, ω and the "temperature-normalized" rupture, t_r as follows

$$\omega(t) = -\frac{1}{\phi}\ln\left[1-\left[1-\exp(-\phi)\right]\frac{t}{t_r}\right] \tag{4.9}$$

$$t_r \exp\left(\frac{-Q_c}{RT}\right) = \left[M \sinh\left(\frac{\sigma}{\sigma_t}\right)^{\chi}\right]^{-1} \tag{4.10}$$

Damage [Eq. (4.9)] depends on the constant ϕ and rupture, t_r. Rupture [Eq. (4.10)] depends on the M , σ_t , and χ material constants.

Assume that initial damage is $\omega_0 > 0$. The "temperature-normalized" MCSR and rupture predictions are reintegrated as

$$\frac{\dot{\varepsilon}_{\min}}{\exp\left(\frac{-Q_c}{RT}\right)} = A_0 \sinh\left(\frac{\sigma}{\sigma_s}\right)\exp(\lambda\omega_o) \tag{4.11}$$

$$t_r \exp\left(\frac{-Q_c}{RT}\right) = \frac{\left[\exp(-\phi)-\exp(-\phi\omega_o)\right]}{M_0 \sinh\left(\frac{\sigma}{\sigma_t}\right)^{\chi}\left[\exp(-\phi)-1\right]} \tag{4.12}$$

where the presence of initial damage will cause the MCSR to increase and rupture time to decrease. Damage with initial damage is also furnished as

$$\omega(t) = -\frac{1}{\phi}\ln\left[\exp\left(-\phi\omega_0\right)-\left[\exp\left(-\phi\omega_0\right)-\exp(-\phi)\right]\frac{t}{t_r}\right] \tag{4.13}$$

where the presence of initial damage causes the damage to increase.

A closed-form creep strain equation can be derived as

$$\varepsilon_{cr} = \frac{\theta\phi\left(\exp\left(\frac{\sigma}{\sigma_s}\right) - \exp\left(-\frac{\sigma}{\sigma_s}\right)\right)}{2(\lambda-\phi)}\left[\Psi - \frac{t+\Psi}{\left(\frac{t_r - t + t\exp(-\phi)}{t_r}\right)^{\frac{\lambda}{\phi}}}\right] \tag{4.14}$$

$$\theta = A_0 \exp\left(-\frac{Q_c}{RT}\right)$$

$$\Psi = \frac{t_r}{\exp(-\phi)-1}$$

This equation, can be employed for $\omega_0 = 0$ or $\omega_0 > 0$ conditions by using the appropriate rupture prediction equation [Eq. (4.10)] or [Eq. (4.12)] respectively. The integration of a closed-form creep strain equation indicates that a closed-form material Jacobian for finite element analysis also exists.

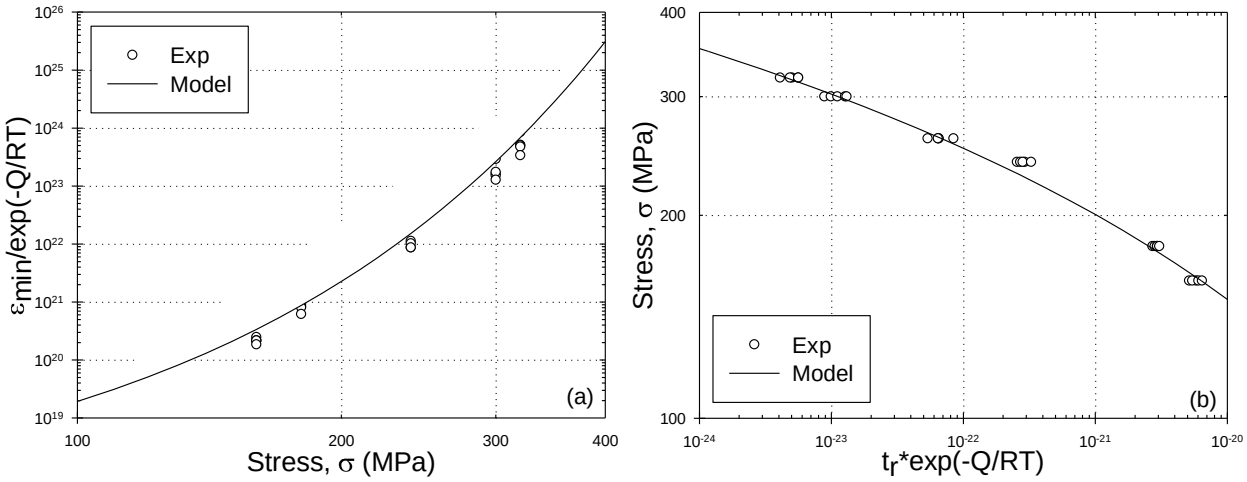

Figure 4.1: Normalized (a) MCSR and (b) SR data and calibrated best-fit model [Eqs (4.3) and (4.10)]

4.2 DETERMINISTIC CALIBRATION

The Sinh calibration begins deterministically. Nine material constants are required $\left(\varepsilon_{pr}, Q_c, A, \sigma_s, M, \sigma_t, \chi, \lambda, \phi\right)$: four are fixed $\left(Q_c, \sigma_s, \sigma_t, \chi\right)$ and five are specimen-specific

$\left(\varepsilon_{pr}, A, M, \lambda, \phi\right)$. The deterministic calibration follows a previously established approach by Haque et al [54]. The normalized MCSR and SR [Eqs. (4.3)-(4.10)] are calibrated through the best-fit in the experimental data to produce the fixed material constants $\left(Q_c, A^*, \sigma_s, M^*, \sigma_t\right)$ listed in Table 4.1. The A^* and M^* constants are the best-fit material constants that pass through the middle of the data. The activation energy, Q_c is comparable to literature [55]. The specimen-specific material constants arise as follows. Specimen-specific A and M constants are back-calculated from [Eqs. (7)-(8)] compared to creep-data to produce perfect MCSR and SR predictions. The λ constant is calculated from the MCSR and FCSR data using [Eq. (4.4)]. The specimen-specific material constant ϕ is numerically optimized using the closed-form creep strain [Eq. (4.14)]. The specimen-specific primary creep strain, ε_{pr} is measured directly from creep data. The specimen-specific material constants $\left(A_0, M_0, \lambda, \phi, \varepsilon_{pr}\right)$ for all thirty creep tests are provided in Table 9.1 of the Appendix.

Table 4.1 : Fixed material constants for Sinh model of alloy 304 SS

Q_c	A^*	σ_s	M^*	σ_t	χ
$(\text{kJ}\cdot\text{mol}^{-1})$	$(\%\cdot\text{hr}^{-1}\times 10^{17})$	(MPa)	$(\text{hr}^{-1}\times 10^{17})$	(MPa)	
419	3.310	21	9.462	66.5	3.0

*these are the best-fit material constants for all the data. The specimen-specific material constants are provided in the Appendix Table 9.1.

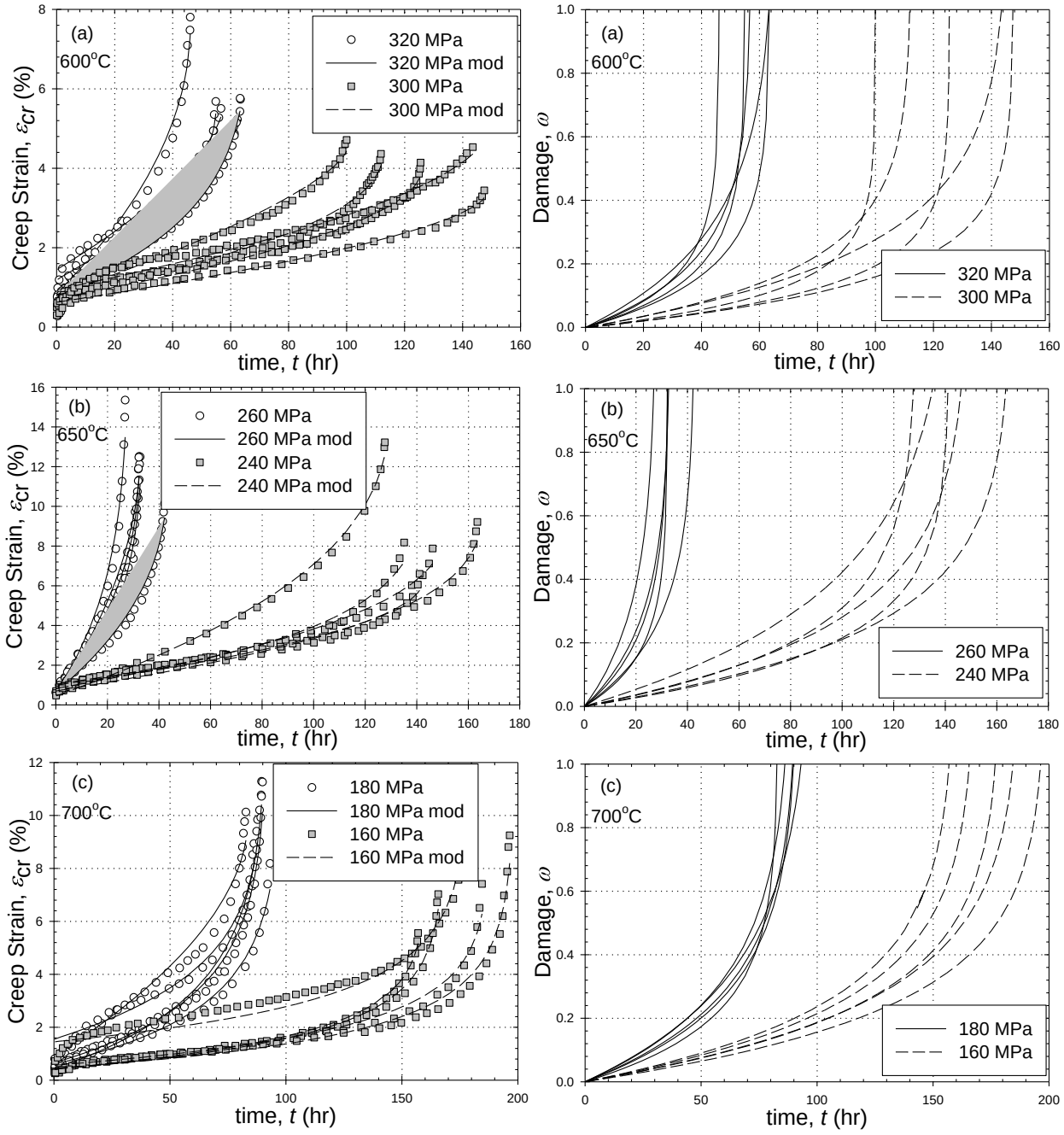

Figure 4.2: Deterministic creep deformation and damage predictions using the Sinh model for 304SS (a) 600°C at 300 and 320 MPa, (b) 650°C at 260 and 240 MPa, and (c) 700°C at 180 and 160 MPa

The Creep deformation and damage predictions using the specific-specimen constants are shown in Figure 4.2. Qualitative and quantitatively, the model is highly accurate with a mean % Error in MCSR of 10.433%. The mean %Error in creep ductility is low at 8.978%. The SR predictions perfectly match the data. The %Error statistics of MCSR and creep ductility is shown in Table 4.2. Critical damage is always unity. These deterministic predictions represent the case where uncertainty is carried 100% by the specimen-specific material properties.

Table 4.2 : Percent Error % in Deterministic MCSR and Creep Ductility Predictions

Parameter	Max	Min	Mean	Std Dev	CoV
MCSR	17.100	2.493	10.433	3.245	31.107
Ductility	15.533	3.274	8.978	2.817	31.378

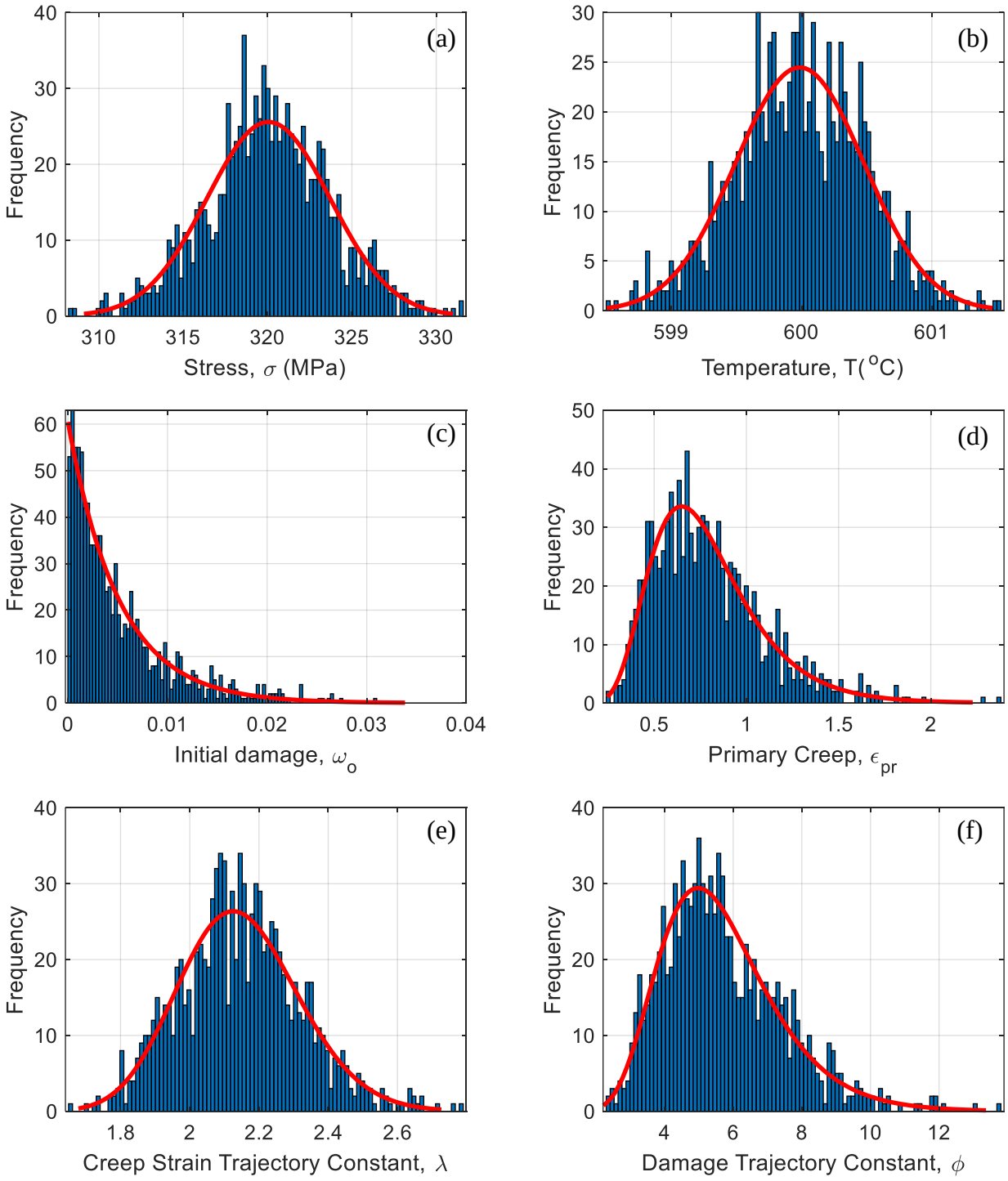

Figure 4.3: Probability distribution functions (pdfs) for (a) stress, σ (b) temperature, T (c) initial damage, ω_0 (d) primary creep strain, ε_{pr} (e) creep strain trajectory constant, λ, and (f) damage trajectory constant, ϕ. These set of pdfs are for case 320 MPa at 600°C.

4.3 PROBABILISTIC CALIBRATION

The probabilistic calibration process and model employs the Sinh equations with initial damage [Eqs. (4.11)-(4.13)]. The previously determined fixed material constants $\left(Q_c, A^*, \sigma_s, M^*, \sigma_t\right)$ are preserved. Scatter in the experimental data is calibrated into the model by defining probability distribution functions (pdfs) for the test conditions (σ and T), initial damage, ω_0, and material constant $\left(\varepsilon_{pr}, \lambda, \phi\right)$ uncertainty. Note, these uncertainties are not co-calibrated; rather, they are individually applied to the data and then aggregated together once the full probabilistic model is enabled. The calibrated pdfs are shown in Figure 4.3 and their parameters are summarized in Table 4.3. The Matlab distribution fitter app and/or Anderson-darling (AD) goodness-of-fit test are employed to identify and calibrate the pdfs. The probabilistic parameters conform to ASTM standards, CDM rules, and the nature of the specimen-specific constants. A monograph of the calibration process follows.

Table 4.3 : Probability distributions shapes and parameters for probabilistic prediction

Parameter	Distribution Shape	Distribution Parameters
σ	Normal Gaussian	$\mu = X$ MPa*, $\sigma = (0.046 \times \mathrm{X} + 0.006) / 4$ MPa
T	Normal Gaussian	$\mu = X\,°C^*$, $\sigma = 4°C / 8$
ω_0	Exponential	$\mu = 0.005$
ε_{pr}	Lognormal	$\mu = -0.309$, $\sigma = 0.362$
λ_0	Lognormal	$\mu = 1.664$, $\sigma = 0.084$
ϕ_0	Lognormal	$\mu = 0.971$, $\sigma = 0.289$

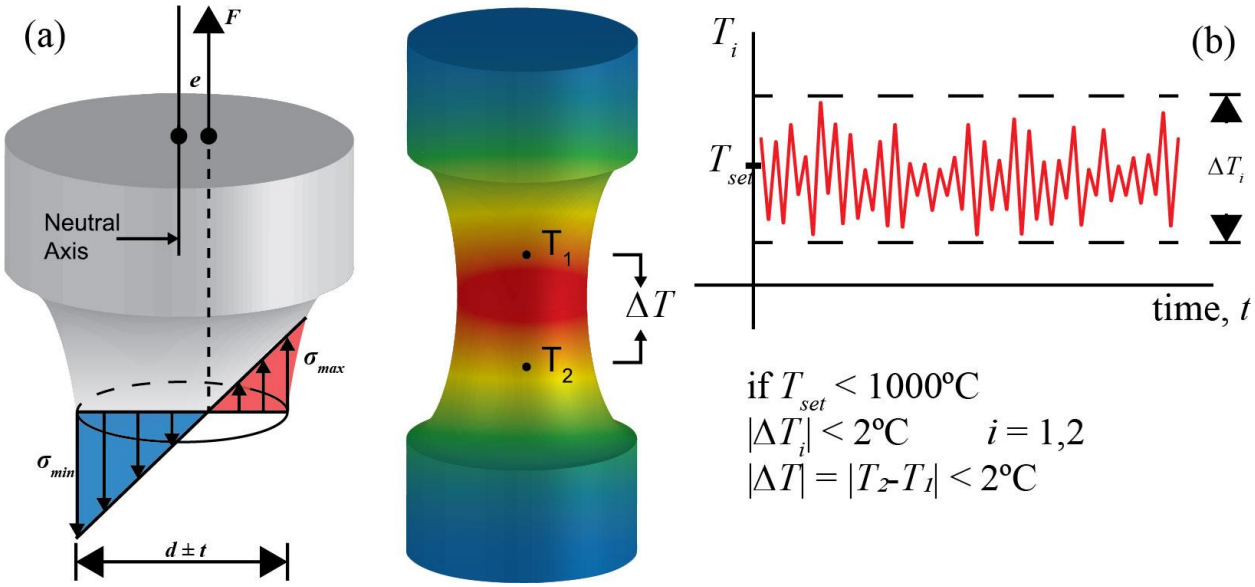

Figure 4.4: Illustration of (a) eccentric loading and (b) temperature fluctuations during a creep test. Herein, $\sigma_{max}, \sigma_{min}$ - Maximum and minimum normal bending stress, F - Applied load, t - tolerance in dimensions relative to neutral axis, e - eccentricity of loading, and T_i - Temperature recorded from thermocouple.

Test condition uncertainty can usually be calibrated by measuring the eccentricity of the specimen and load frame and examining thermocouple data. In this study, that information is not available; therefore, to be conservative, the worst-case scenario allowed under ASTM standards is applied. Stress and temperature uncertainties are idealized in Figure 4.4. Stress fluctuations arise from the eccentric loading of a specimen due to the misalignment of the load-frame and/or dimensional tolerance. The ASTM E8 standard calls for a stress increase of 1.5, 2.5, and 3.2% for 12.5, 9, and 6 mm diameter specimens respectively when eccentricity is held to 0.025 mm [56]. In this study, the specimens have a diameter of 6 ± 0.025 mm, thus the worst-case scenario is +3.2% stress. Stress uncertainty is applied using Normal Gaussian pdf where the mean is equal to nominal stress and the standard deviation is equal to 1/4th of a linear function (0.046 × mean stress + 0.006)

as shown in Figure 4.3(a). The chosen pdf is appropriate because more than 95% of the distribution is captured within the $\pm 3.2\% \sigma$ bands. A more elaborate formula for adding stress uncertainty could be derived by using solid mechanics to solve for the stress increase caused by the interaction of load/geometric eccentricity, concentricity of the specimen gauge section and the load-frame, and load-frame misalignment as illustrated in Figure 4.4(a) information is not available to implement it here.

Temperature fluctuations arise during creep testing and exhibit both spatial (along the specimen gauge-length) and temporal properties. The ASTM E139 standard states that temperature must not fluctuate more than ±2°C below 1000°C and ±3°C above 1000°C duration of testing [44]. Furthermore, since two thermocouples are required, fluctuations must remain below this limit at each location and between them, respectively. In this study, the specimens are subjected to temperatures below 1000°C, thus the worst-case scenario is ±2°C temperature. Temperature uncertainty is applied using a Normal Gaussian pdf where the mean is equal to nominal temperature and the standard deviation is equal to 1/8th of the temperature range as shown in Figure 4.4(b). The chosen pdf is appropriate because 100% of the distribution is captured within the ±2°C bands.

Initial damage, ω_0 is influenced by residual stresses [40], pre-existing cavities and defects [57-60], and loading history including the monotonic loading need to reach the creep load [61-63]. Rather than evaluate these sub-sources of uncertainty, a collective approach is applied where the remaining uncertainty in the SR data is eliminated by adding initial damage. Note, the MCSR data is not employed to calibrate initial damage. It will be shown in the following section that, given a fixed λ and ϕ, initial damage has marginal impact on MCSR unless the magnitude of initial

damage values are large $|\omega_o| > 0.2$. Conversely, changing λ and ϕ has minimal impact on the SR predictions.

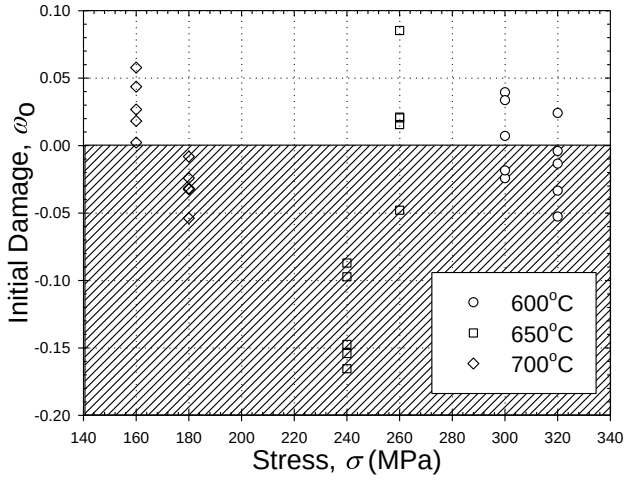

Figure 4.5: Initial damage, ω_0 versus stress calculated employing the specimen-specific λ and ϕ to obtain specimen-specific ω_o from the SR data

Initial damage, ω_0 is obtained for each data point by applying the specimen-specific ϕ constants (that were obtained when $\omega_0 = 0$) and rearranging the rupture equation [Eq. (4.12)] to solve for initial damage. The resulting initial damage, ω_0 versus stress is plotted in the Figure 4.5. A trend of initial damage with stress or temperature is not observed; suggesting that the calculated values are free of stress- and temperature-dependence. Positive (n=13) and negative (n=17) initial damage values are calculated. In the deterministic calibration, [Eq. (4.2)] is employed to calibrate the specimen-specific constants for a perfect fit to SR data where the initial damage is zero. In the probabilistic calibration, the same specimen-specific constants are used but for non-zero initial damage [Eq. (4.12)]. To preserve accuracy, often the initial damage becomes negative. Negative damage, $\omega_0 \leq 0$ violates CDM [64]. To be conservative and meet CDM rules, the $\omega_0 \leq 0$ values are discarded. Discarding $\omega_0 \leq 0$, the average ω_0 is 0.01. The MATLAB distribution fitter app is

employed to determine the distribution parameter of the chosen pdf. In the probabilistic model, the uncertainty for ω_0 is set between 0 to 0.01 with an exponential distribution and the distribution parameter mean, $\mu = 0.005$ as shown in Figure 4.3(c). The chosen pdf is appropriate because the specimens are likely to be virgin with minimum initial damage. Densitometry techniques can also be employed to estimate initial damage by measuring the bulk porosity and/or the local void volume fraction within the microstructure before testing [61-63].

The uncertainty of ε_{pr} is based on the specimen-specific values. The measured ε_{pr} do not trend with stress or temperature. Uncertainty of ε_{pr} is applied using a Lognormal pdf where the mean and standard deviation are equal to -0.309 and 0.362 respectively as shown in Figure 4.3(d). The Anderson-Darling (AD) goodness-of-fit test statistics were employed to identify and calibrate the pdf. In the future, a multistage Sinh model could be employed [64].

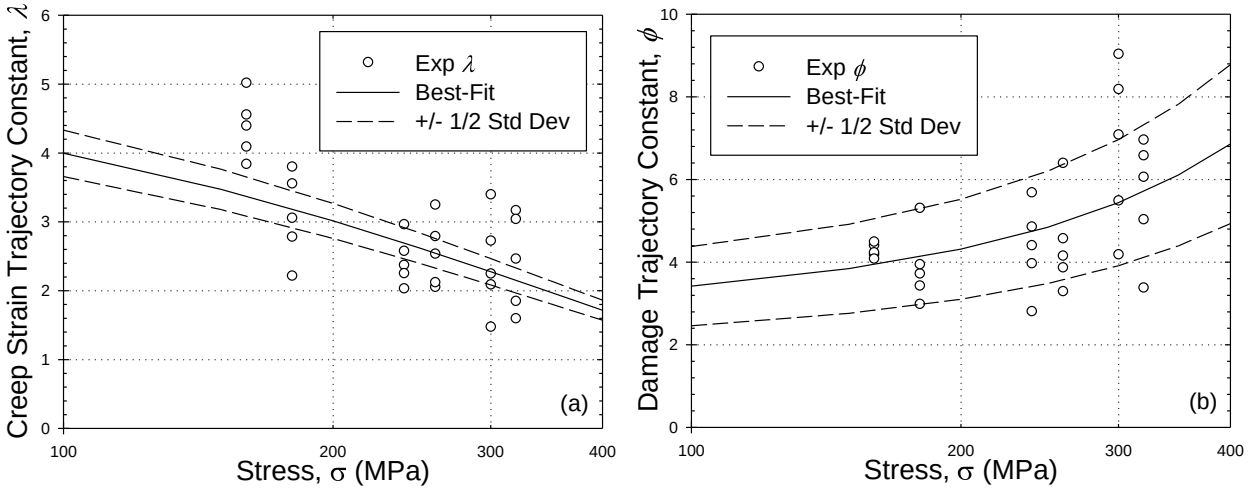

Figure 4.6: Eyring prediction [Eq. (4.7) and (4.8)] of the specimen-specific constant λ and ϕ versus stress. The solid line is the best fit. The dashed line represents ±1/2 standard deviation.

The uncertainty of λ and ϕ is established based on the specimen-specific constants. Eyring predictions [Eqs. (4.7) and (4.8)] of λ and ϕ are plotted versus stress in Figure 4.6. Best-

fits are obtained by numerically optimizing the coefficients (λ_0 and ϕ_0) and activation volumes (V_λ^* and V_ϕ^*) as reported in Table 4.4. The standard deviation of the specimen-specific λ and ϕ are 0.892 and 1.523 respectively. The dashed lines are obtained by taking the best-fit constants (λ_0 and ϕ_0) ± 1/2 standard deviation. The uncertainty of λ and ϕ are set with a Lognormal distribution as shown in Figure 4.3(e)-(f) respectively. The pdfs were selected based on Anderson-Darling (AD) goodness-of-fit test.

Table 4.4 : Eyring's constants for λ and ϕ

Parameter	Coefficient	Activation Volume (10^{-23}cm^3)
λ [Eq. (4.7)]	5.295	3.392
ϕ [Eq. (4.8)]	2.715	2.795

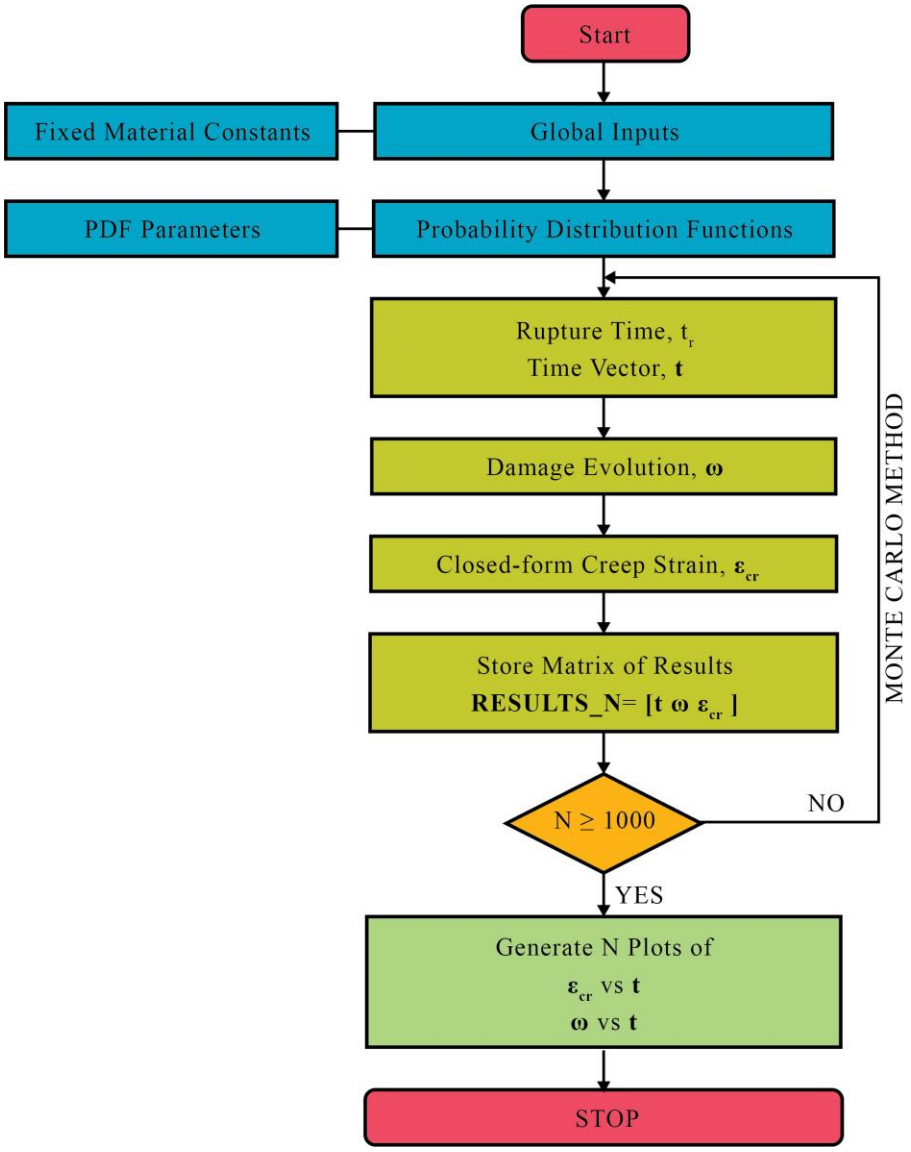

Figure 4.7: Flowchart of Sinh model creep deformation and damage prediction using Monte Carlo sampling method

4.4 MONTE CARLO SAMPLING

A MATLAB subroutine is developed to generate probabilistic Sinh model predictions. The flowchart is illustrated in Figure 4.7. The global inputs of the subroutine are the fixed material constants $\left(Q_c, A^*, \sigma_s, M^*, \sigma_t\right)$ and Eyring constants reported in Table 4.1 and Table 4.4

respectively. Monte Carlo sampling is applied to the $(\sigma, T, \varepsilon_{pr}, \omega_0, \lambda_0, \phi_0)$ pdfs reported in Table 4.3 to generate 1000 unique creep deformation and damage evolution predictions. First, 1000 rupture times, t_r [Eq. (4.12)] are predicted. The predicted rupture times, t_r are divided by 100 to create unique time vectors, $\mathbf{t}$. The closed-form damage and creep deformation equations [Eqs. (4.13)-(4.14)] are employed in conjunction with time vectors, $\mathbf{t}$ to predict the damage evolution, $\boldsymbol{\omega}$ and creep strain, $\boldsymbol{\varepsilon}_{\mathbf{cr}}$ at each iteration. The results are stored in a RESULTS matrix. Thus, 1000 unique creep deformation and damage evolution curves are generated.

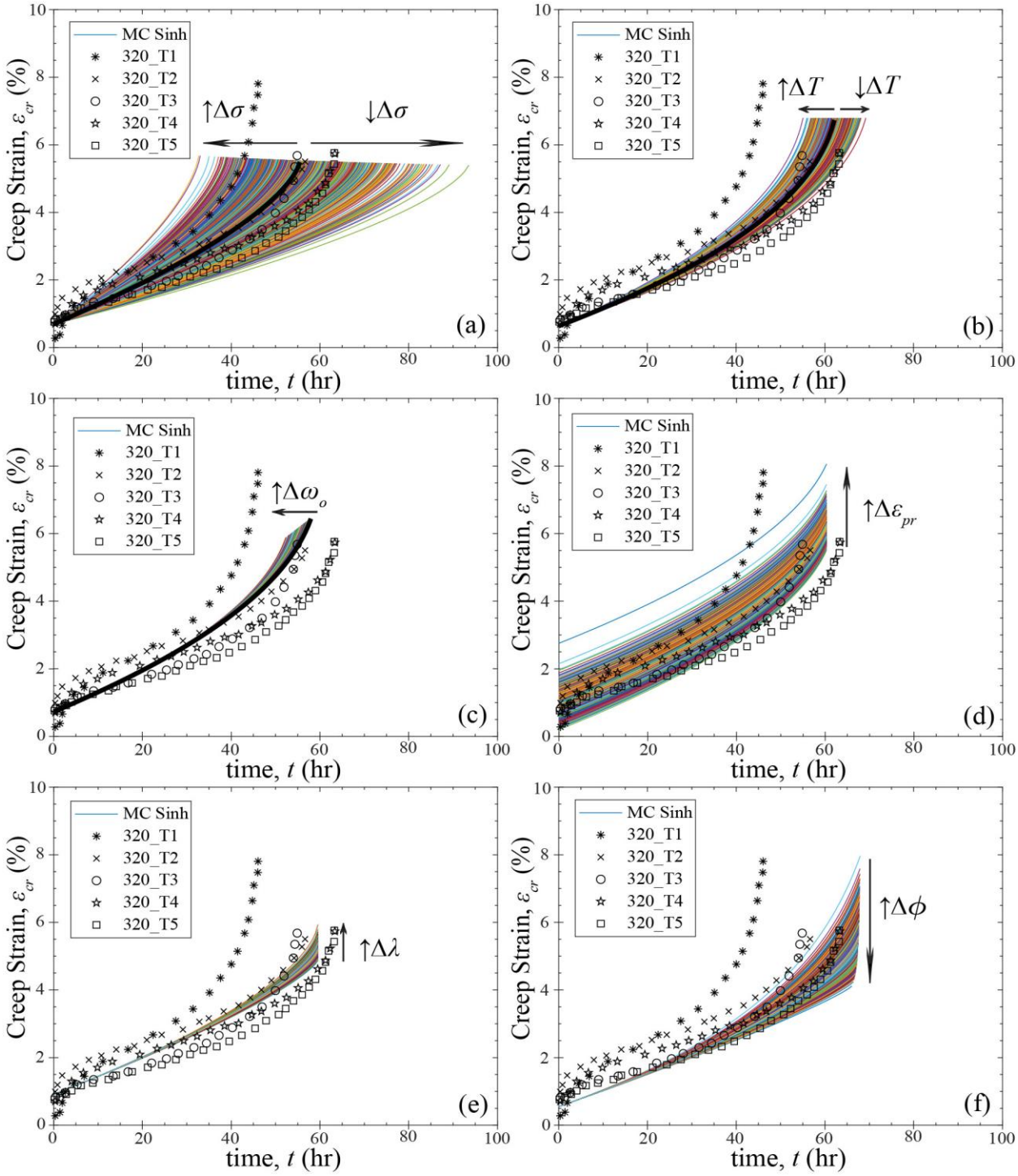

Figure 4.8: Probabilistic creep deformation curves for single source of uncertainty: (a) stress, σ (b) temperature, T (c) initial damage, ω_0 (d) primary creep, ε_{pr} (e) creep strain trajectory constant, λ , and (f) damage trajectory constant, ϕ uncertainty at 320 MPa and 600°C. 1000 Monte Carlo simulations were performed for each source.

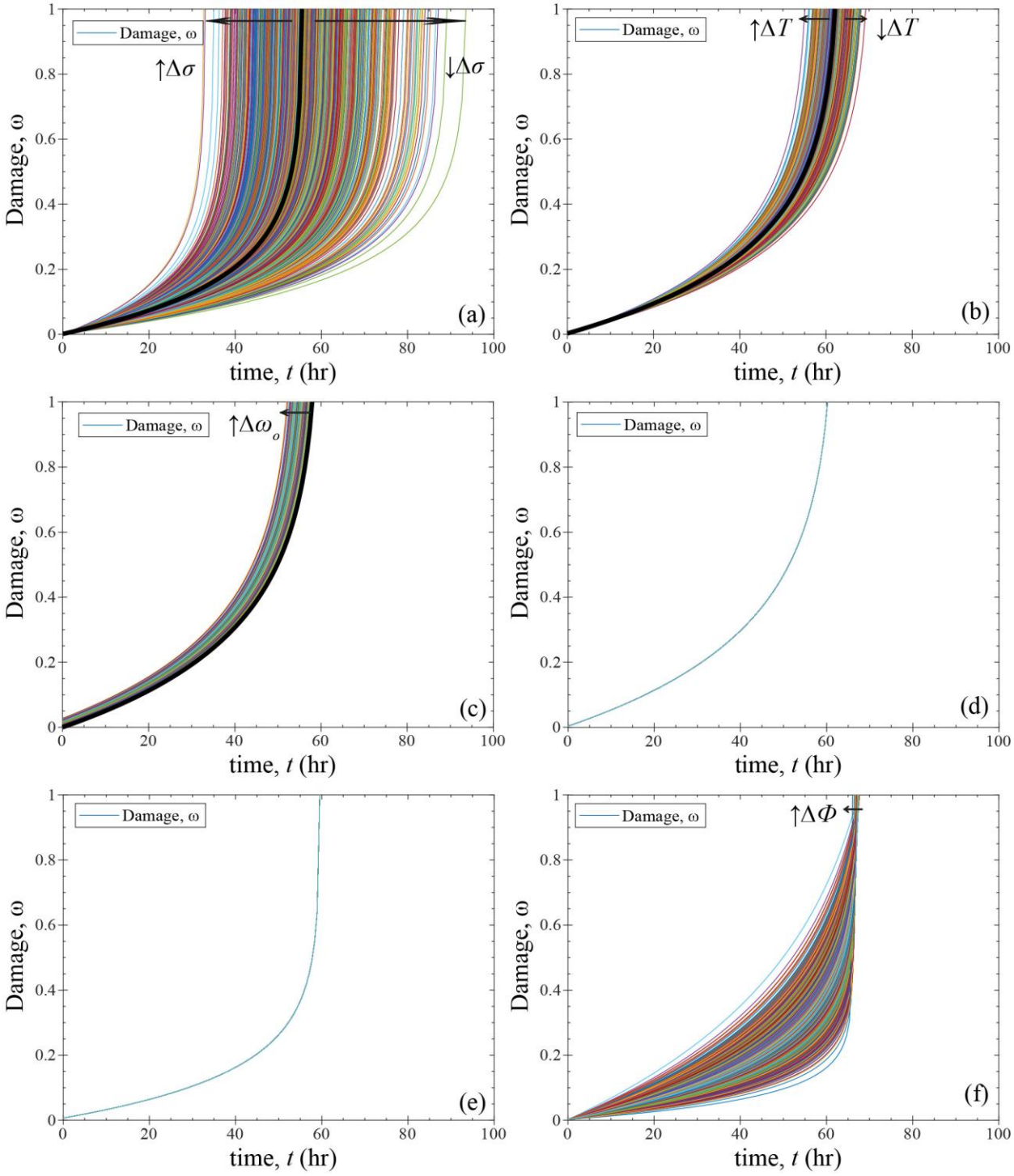

Figure 4.9: Probabilistic damage evolution curves for single source of uncertainty: (a) stress, σ (b) temperature, T (c) initial damage, ω_0 (d) primary creep, ε_{pr} (e) creep strain trajectory constant, λ , and (f) damage trajectory constant, ϕ uncertainty at 320 MPa and 600°C. 1000 Monte Carlo simulations were performed for each source.

4.5 PROBABILISTIC PREDICTION: INDIVIDUAL SOURCE

Individual source predictions are performed by turning on each source of uncertainty individually. The influence of that source of uncertainty on creep deformation and damage evolution is evaluated. For brevity, only the creep deformation and damage predictions corresponding to the 320 MPa and 600°C creep data are evaluated. The creep deformation predictions are shown in Figure 4.8. The black solid lines represent the nominal state where stress and temperature are exact and initial damage is zero. Qualitatively, increasing stress and temperature shifts forward the creep deformation curve reducing the rupture time as shown in Figure 4.8(a) and Figure 4.8(b). This is expected from literature [65-66]; however, only a token increase of creep ductility is observed, and it is restricted to stress increases only. The effect of stress is more pronounced than temperature. In addition, the MCSR increases with stress but not temperature. Adding initial damage, ω_0 decreases both creep ductility and rupture as shown in Figure 4.8(c). Adding or decreasing primary creep, ε_{pr} shifts the creep deformation curve up and down respectively as shown in Figure 4.8(d). Increasing the creep strain trajectory constant, λ increases creep ductility with negligible impact on rupture as shown in Figure 4.8(e). Increasing the damage trajectory constant, ϕ decreases creep ductility and rupture as shown in Figure 4.8(f).

The damage evolution predictions are shown in Figure 4.9. Meeting CDM rules, damage is always unity at rupture as shown in Figure 4.9(a)-(f) [64]. Qualitatively, increasing stress, temperature, and initial damage shifts the damage curve forwards reducing rupture time as shown in Figure 4.9(a)-(c) respectively. Again, the effect of stress is the most pronounced. Primary creep, ε_{pr} and the creep strain trajectory constant, λ have no impact on damage evolution as shown in Figure

4.9(d)-(e) respectively. Increasing the damage trajectory constant, ϕ causes the damage evolution curve to exhibit a sharper trajectory with a shorter rupture time as shown in Figure 4.9(f).

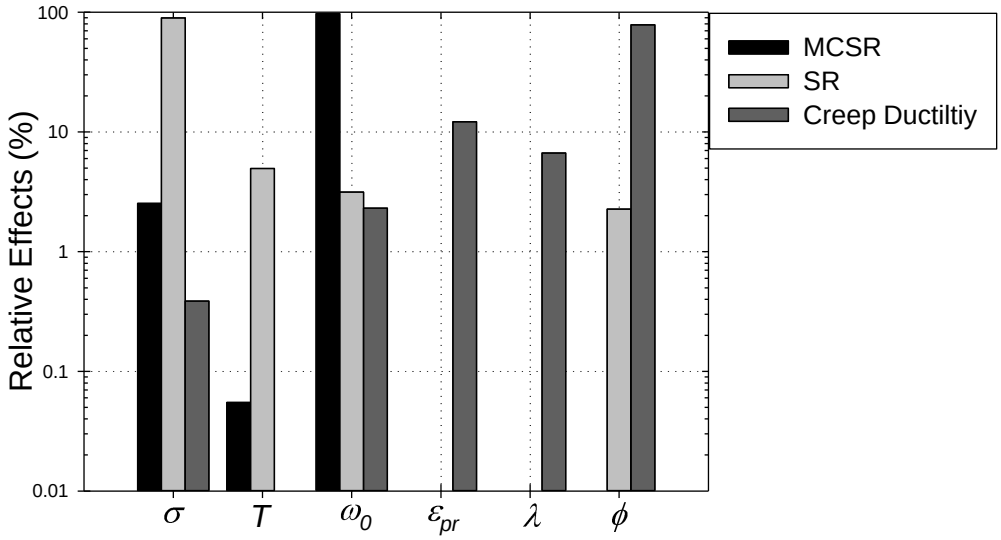

Figure 4.10: Analysis of variance (ANOVA) of individual parameters on MCSR, SR, and creep ductility prediction.

A quantitative analysis is performed on the sources of uncertainty using the analysis of variance approach (ANOVA). This analysis is restricted to the influence of individual sources on the predicted MCSR, SR, and creep ductility as shown in Figure 4.10. The Relative Effect (%) expresses the influence of one source relative to other sources in an assessment. The MCSR, SR, and creep ductility are most influenced by initial damage, stress, and the damage trajectory constant, ϕ respectively at 97.410, 89.631, and 78.444% of relative effect. Temperature most influences SR at 4.944%. The primary creep strain and creep strain trajectory constant, λ solely influence the creep ductility at 12.169 and 6.686% respectively.

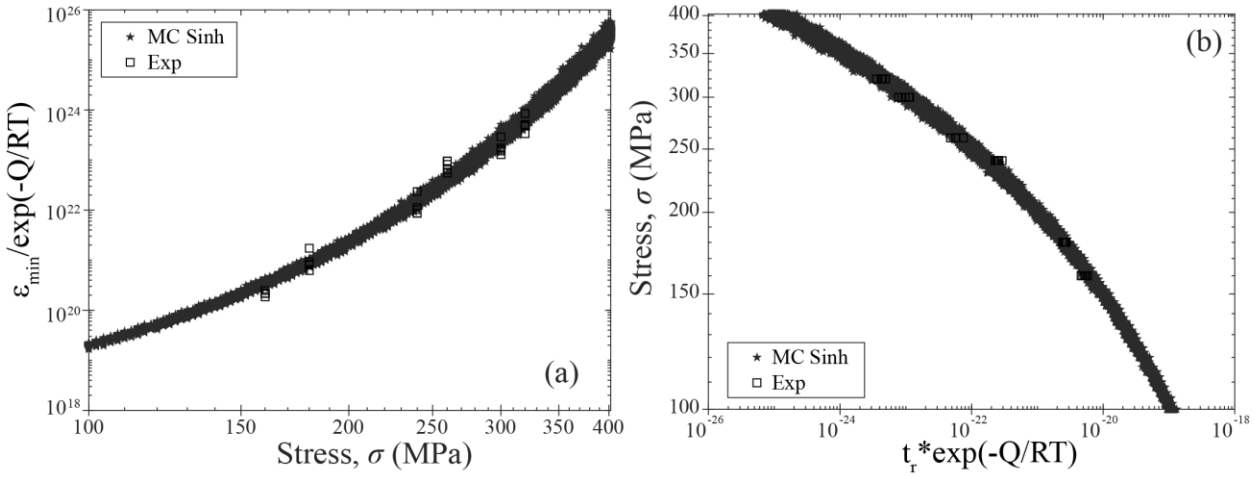

Figure 4.11: Normalized (a) MCSR and (b) SR predictions using the full interaction model

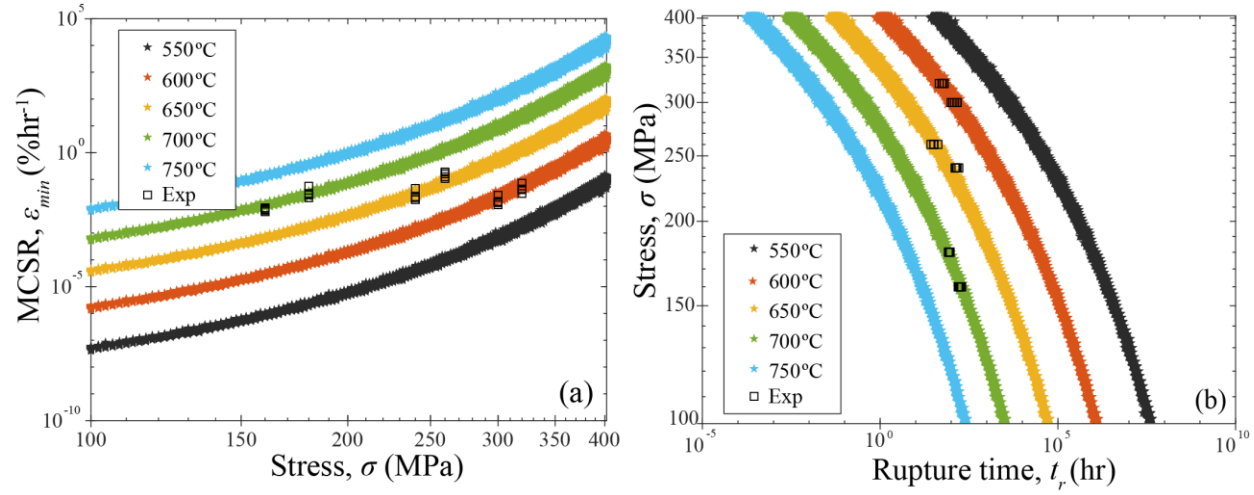

Figure 4.12: Predicted (a) MCSR and (b) SR bands across multiple isotherms using the full interaction model.

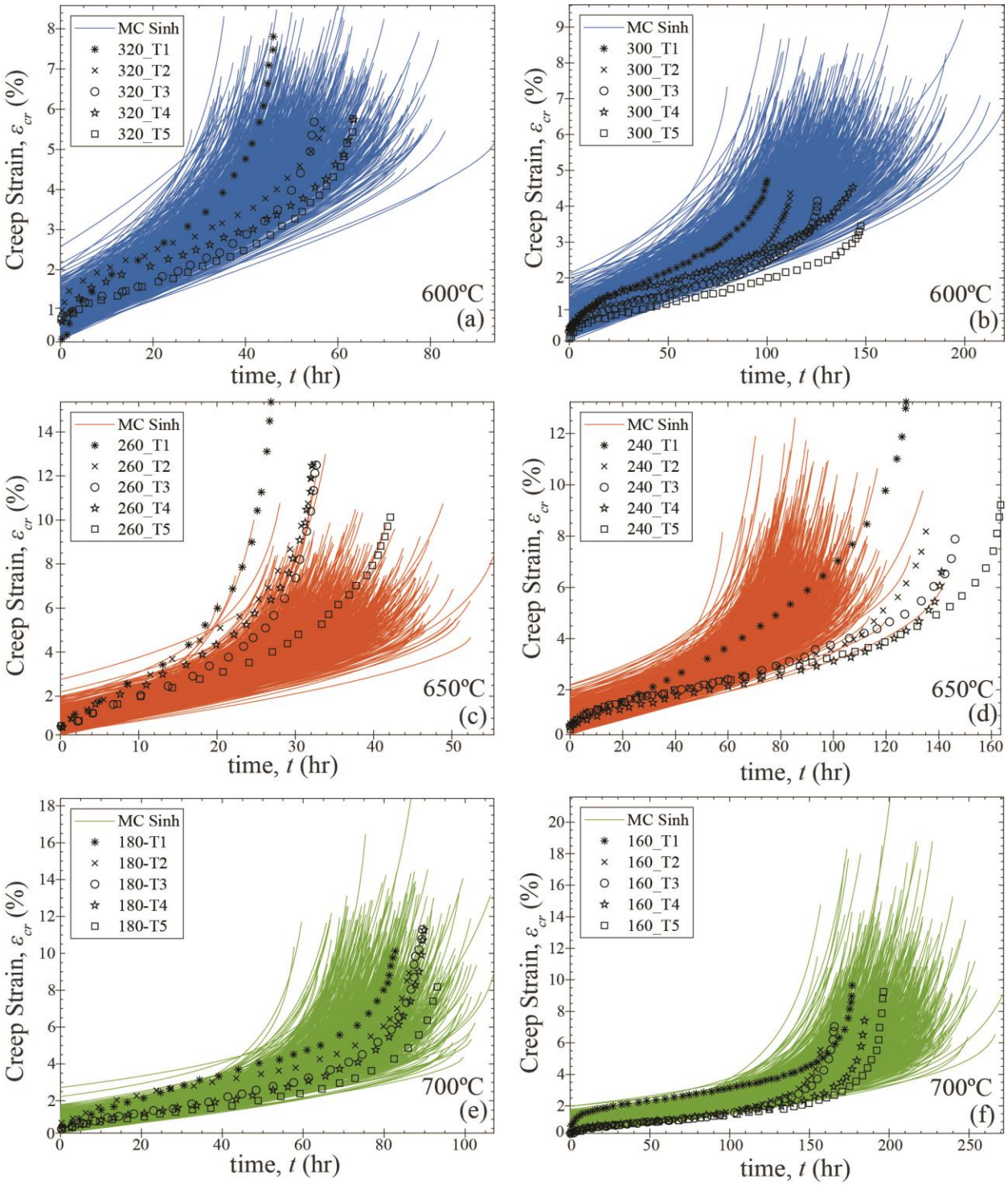

Figure 4.13: Creep deformation curves using the full interaction model at 600°C subjected to (a) 320 MPa and (b) 300 MPa, at 650°C subjected to (c) 260 MPa and (d) 240 MPa, and at 700°C subjected to (e) 180 MPa and (f) 160 MPa respectively. 1000 Monte Carlo simulations for each condition.

4.6 PROBABILISTIC PREDICTION: FULL INTERACTION

The full interaction simulations are performed where the fidelity of the full probabilistic model is evaluated. In these simulations all source of uncertainty are "turned on". The "Normalized" MCSR and SR predictions are shown in Figure 4.11(a)-(b). The goodness-of-fit of the MCSR and SR predictions are satisfactory. The predictions cover the bounds of the experimental data (across isostress-isotherm conditions). The isotherms can be better examined individually in the Figure 4.12(a)-(b) where the predictions agree with the experimental data at each isotherm. The extrapolated MCSR and SR predictions, show a narrowing band at low-stress and a constant bandwidth with respect to temperature. This is opposed to creep theory where scatter is expected to increase in the low-stress high-temperature regime primarily due to the additional energy and time allowing for stochastic metallurgical processes and time-temperature-transformation (TTT) and precipitation (TTP) [68-69]. Mathematical analysis was performed to identify the root cause. It was determined that the deterministically measured damage trajectory constant, ϕ, (N=30) increases with stress as shown Figure 4.6(b) which is opposed to previous studies on alloy 18Cr-12Ni-Mo (N=322) [70]. Ultimately, the probabilistic model is only as good as the quality and quantity of data employed in calibration. A lack of low-stress high-temperature data, results in the model incorrectly extrapolating that regime. Future investigations can further improve the model by: (a) employing a higher quality and quantity of data during calibration; (b) applying stochastic time-dependent probability distribution functions (pdfs) which expand as a function of time; and (c) incorporating TTT and TTP diagrams (experimentally- or CALPHAD-derived) into the calibration and modeling process.

The creep deformation predictions of the experimental data are shown in Figure 4.13(a)-(f). The goodness-of-fit with the experiment across multiple isostress-isotherm is satisfactory.

Qualitatively, the predictions at 600 and 700°C matches the MCSR, SR, and creep ductility of the experiment. At 650°C, the prediction at 260MPa underpredicts creep ductility while at 240 lacks in accurate rupture prediction. The underlying cause of shorter ductility and rupture prediction are the fixed material constant, A^* and M^*, respectively. At 260 MPa, the average specimen-specific A_0 is 100% higher than A^*. At 240 MPa, the average specimen specific M_0 is 39% lower than M^*. The resulting effect is seen in the shorter creep ductility and rupture prediction. Herein, 1000 Monte carlo simulation is performed per test condition as further simulation does not improve the accuracy of the prediction.

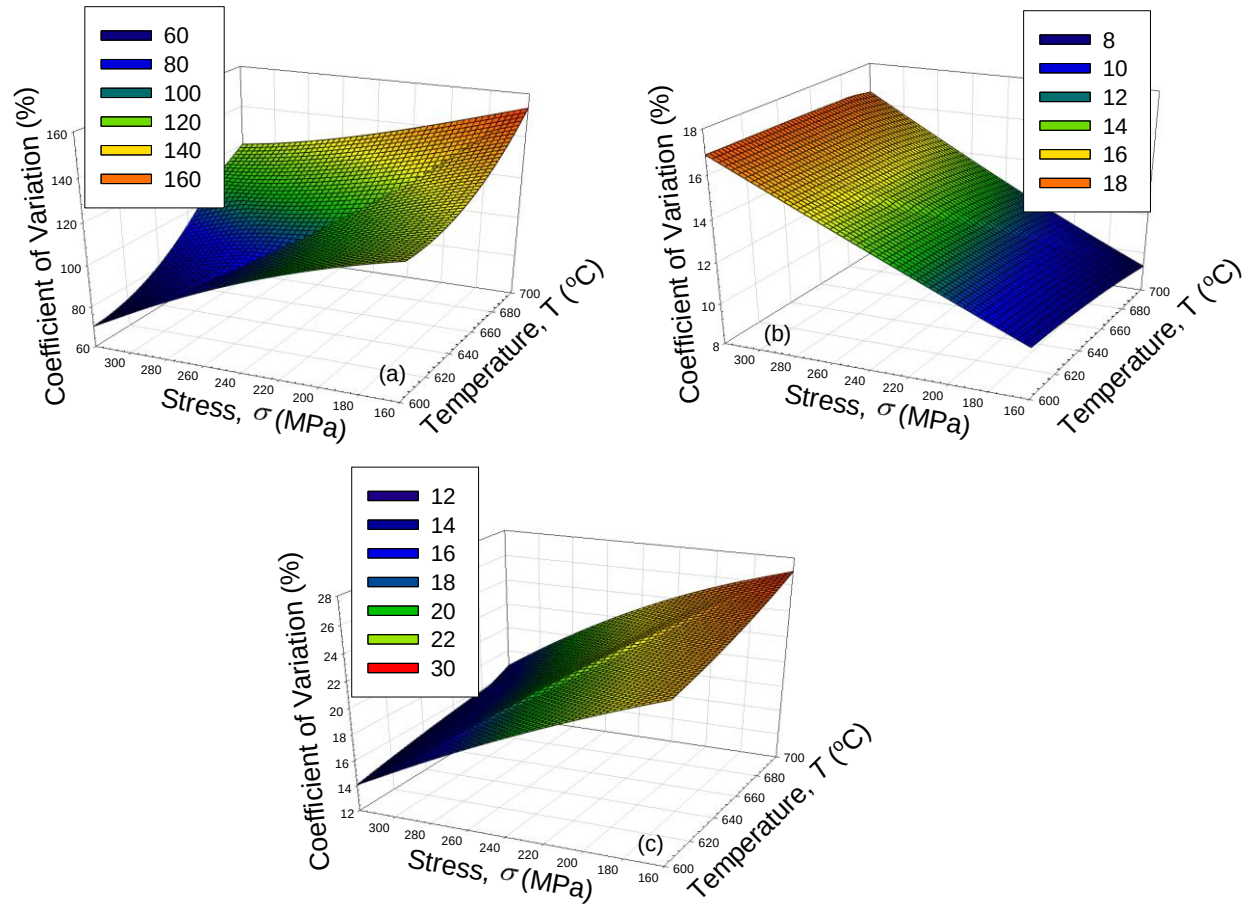

Figure 4.14: Coefficient of variation (CoV) of predicted (a) MCSR, (b) SR, and (c) creep ductility at 320-160 MPa and 600-700°C

The coefficient of variation (CoV) of predicted MCSR, SR, and creep ductility across multiple isostress-isotherm is shown in Figure 4.14. At constant temperature, the predicted MCSR and creep ductility variation decrease with stress as shown in Figure 4.14(a) and Figure 4.14(c) respectively. On the contrary, the predicted rupture variation increases with stress as shown in Figure 4.14(b). The predicted MCSR and creep ductility show increasing trend with temperature while the opposite is noticed for predicted rupture. The observed variation is more appreciable for stress than temperature. As low stress – high temperature regime approach, the variation is significant.

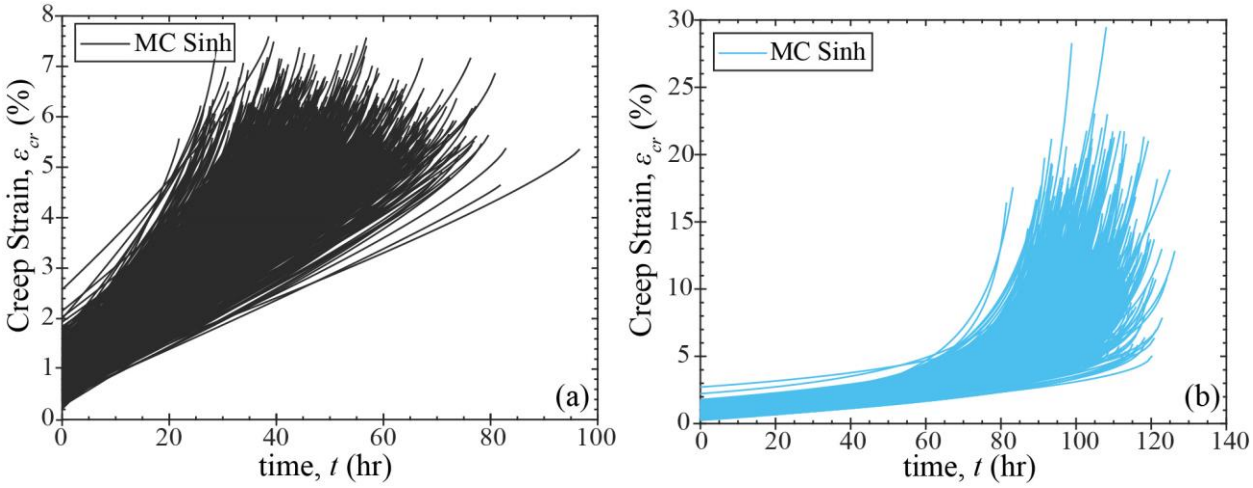

Figure 4.15: Extrapolation of the creep deformation using the full interaction model at (a) 400 MPa and 550°C and (b) 120 MPa and 750°C respectively.

To further evaluate the extrapolation ability of the model, probabilistic simulations are performed at 400 MPa and 550°C and at 120 MPa and 750°C as shown in Figure 4.15. The extrapolated predictions exhibit the expected creep response trends. The prediction at 400 MPa show shorter MCSR and SR with more scattering while at 120 MPa show longer, consistent, and less scatter. The prediction at 120 MPa exhibit significantly higher creep ductility with more

scattering compared to 400 MPa. The relative scatter bands in MCSR and SR tends to decrease at low-stress matching the “normalized” MCSR and SR prediction.

Chapter 5: Verification and Validation

5.1 INTRODUCTION

The objective of Chapter 5 is the Verification and Validation (V&V) of the probabilistic Sinh prediction described in the preceding chapters. To accomplish the objective, the following steps are undertaken. For deterministic validation, FEA simulation is performed in ANSYS APDL employing a user creep subroutine (USERCREEP.f), an ANSYS user-programmable feature (UPF) for 1D and 2D geometry. The simulated creep deformation and damage evolution for 1D and 2D elements are compared with experiment and deterministic Sinh prediction. For probabilistic prediction, an expanded database of engineering alloys is gathered from NIMS (National Institute for Material Science) and probabilistic model is applied. The probabilistic model is validated by comparing the "Normalized" MCSR and SR prediction. The accuracy of the deterministic and probabilistic result demonstrates the verification and validation of the proposed model. For brevity, the experiment at 320 and 300 MPa at 600°C are accomplished in this chapter.

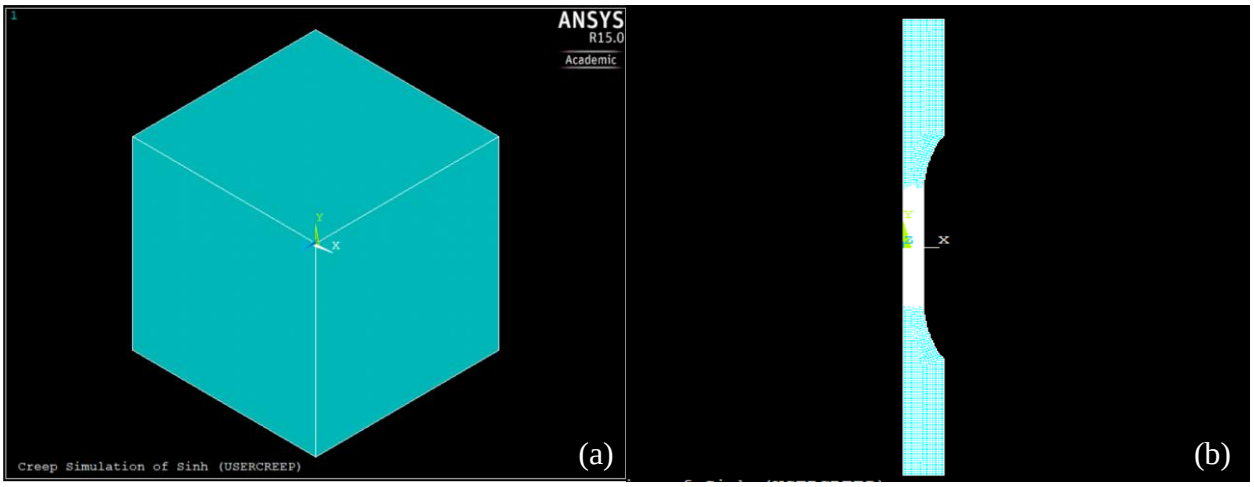

Figure 5.1: Simplified geometry of (a) 1D and (b) 2D models for simulation in ANSYS.

5.2 FEA MODELS: 1D AND 2D

For simplification of the analysis, smooth creep specimen is simulated by simplifying the geometry to a single element 1D and 2D model. The geometry for 1D and 2D model are shown in Figure 5.1. The Young's Modulus and Poisson ratio are taken as $E = 2.65\times10^5$ MPa and $\nu = 0.33$, respectively. For 1D geometry, SOLID185 elements are chosen. Number of nodes per element is 8 and total number of elements is 1. For 2D geometry, eight node PLANE183 elements with plane stress option are chosen. Total number of the elements is 3890. A uniform load according to test condition is applied on the top surface. Appropriate displacement constraints are applied to replicate the uniaxial stress state. The constitutive equations are implemented into USERCREEP UPF. For every Newton-Raphson iteration and material integration point, the USERCREEP UPF is called. At the beginning of the time increment, the inputs are current stresses, strains, and state variables. The USECREEP provide the updated stresses, strains, state variables, and the material Jacobian matrix as outputs [67]. Note that, the Sinh rate-based creep strain [Eq. (4.1)] and damage [Eq. (4.2)] equation are employed. The critical damage is set at unity.

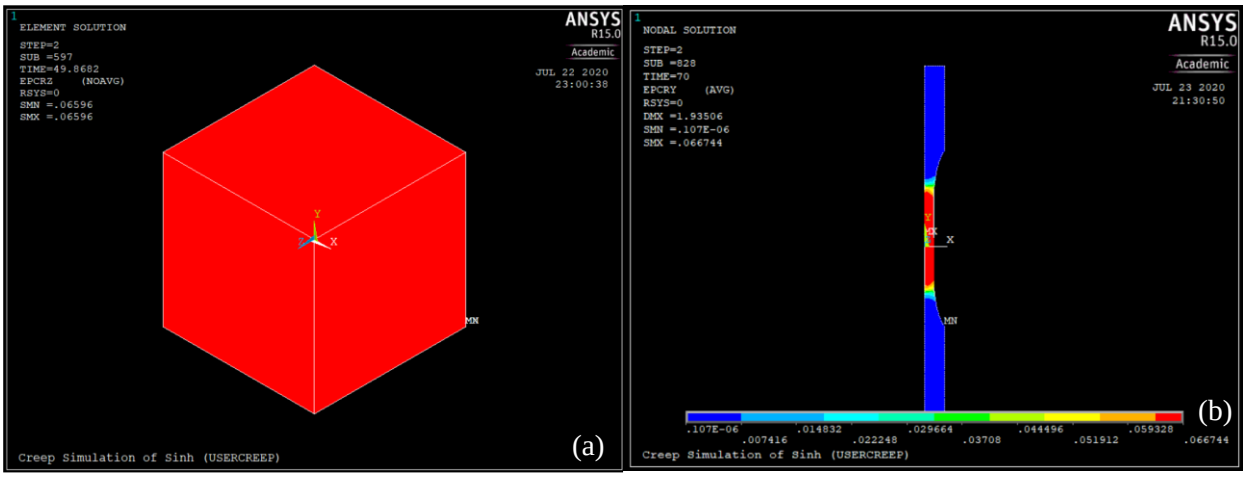

Figure 5.2: Simulated creep strain for (a) 1D and (b) 2D model geometry at 320 MPa at 600°C.

The simulation is run up to the experimental rupture time to facilitate comparison with experimental data. The Sinh material constants summarized in Table 9.1 are employed for the simulation.

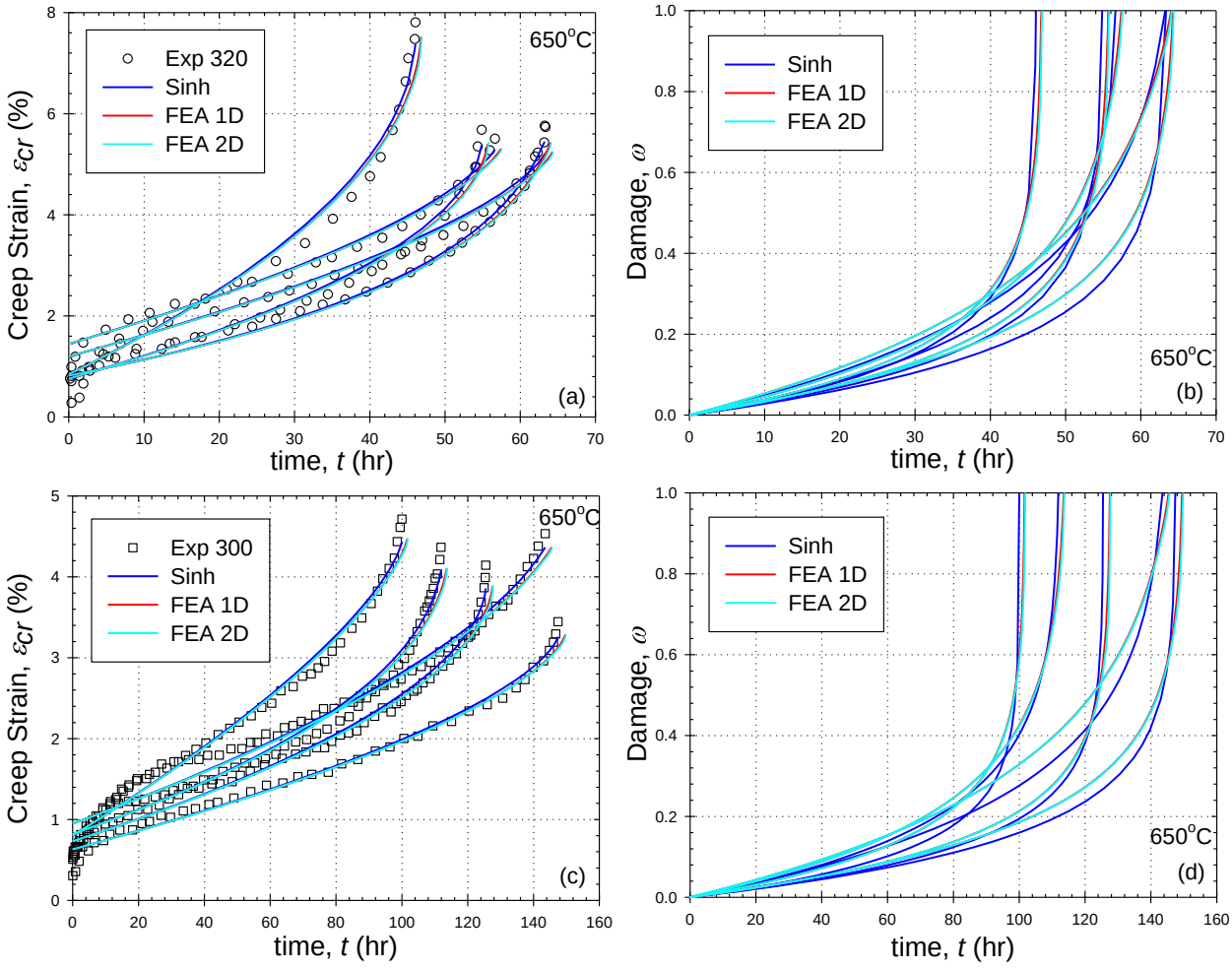

Figure 5.3: Deterministic (a) and (c) creep deformation, and (b) and (d) damage evolution prediction by FEA simulation subjected to 320 and 300 MPa at 600°C.

5.3 Deterministic Prediction: FEA Model

The creep deformation and damage evolution employing the deterministic Sinh material constants are compared with the experiment and deterministic Sinh prediction. A representative simulation of creep strain for 1D and 2D model preformed at 320 MPa and 600°C are shown in

Figure 5.2(a)-(b) respectively. For each test condition, elastic strain, creep strain, and damage evolution is calculated and stored. The deterministic creep deformation and damage evolution prediction by FEA simulation for 1D and 2D elements subjected to 320 and 300 MPa at 600°C are compared to experiment and deterministic Sinh prediction as shown in Figure 5.3. Qualitatively, the FEA 1D and 2D simulation show remarkable accuracy compared to experiment as shown in Figure 5.3(a) and (c). The ductility prediction underpredicts while the rupture prediction overpredict slightly compared to experiment. This is due to time-stepping settings inside the FEA simulation. Minimizing the time-stepping will improve the accuracy in the ductility and rupture prediction. Quantitatively, for 1D and 2D simulation mean %Error in creep ductility with experiment is 5.24% and 5.09%. The rupture prediction mean %Error between experiment and simulation is low at 1.50 and 1.66% for 1D and 2D respectively. The creep ductility prediction show more scatter compared to rupture prediction. The %Error statistics for creep ductility and rupture are summarized in Table 5.1. The damage prediction always goes to unity at rupture meeting the CDM laws as shown in Figure 5.3(b) and (d).

Table 5.1 : Error Statistics in FEA simulated creep ductility and rupture predictions.

Type	Parameter	Max	Min	Mean	Std Dev	CoV
FEA 1D	Creep Ductility	8.471	3.544	5.245	1.538	29.145
	Rupture	1.663	1.278	1.501	0.123	8.034
FEA 2D	Creep Ductility	8.474	3.594	5.097	1.481	29.194
	Rupture	1.826	1.413	1.678	0.131	7.973

5.4 PROBABILISTIC PREDICTION: NIMS DATABASE

5.4.1 Material

The material used for verification and validation of the probabilistic approach are Austenitic stainless steel of type 18Cr-8Ni and 18Cr-12Ni-Mo. The creep data was collected from open source NIMS database [71-72]. For 18Cr-8Ni, this database contains 310 SR and 20 MCSR datapoints and for 18Cr-12Ni-Mo, 323 SR and 32 MCSR datapoints. The materials were in tube form with the dimension of 50.8 mm outer diameter, 8 mm wall thickness, and 5000 mm length. The processing steps includes hot extrusion followed by cold drawing and water quenched at 1130°C. The room temperature (approximately 23-25°C) tensile properties are reported in

Table 5.2 : Tensile properties at RT [71-72].

Property	18Cr-8Ni	18Cr-12Ni-Mo
Yield Stress (MPa)	280	224
Ultimate Tensile Strength (MPa)	610	578
% Elongation	67	68
% Reduction of Area	83	81

The specimen for the creep tests were taken longitudinally from the as-received boiler tubes at the middle of wall thickness. The test specimen has the geometry of 6 mm in diameter (tolerance is ±0.01 mm) and 30 mm (tolerance is ±0.1 mm) in gauge length. The creep-rupture tests were conducted as specified in JIS Z 2272 standard. The accuracy of loading was within ±0.5% of the required load.

5.4.2 Deterministic Calibration

The deterministic calibration follows the same approach described in Chapter 4. The calibrated fixed material constants for the alloys are reported in Table 5.3. As there are no full creep deformation curves, an approximation approach is adopted to calibrate the specimen-specific λ and ϕ. This approach is later verified by parametric simulation across multiple isostress-isotherms. FCSR and final damage rate is calibrated by taking the slope at 2/3rd of rupture time of creep strain and damage evolution curves, respectively. MCSR is taken form the creep datasheet [71-72]. The material constant, λ is calibrated through [Eq. (4.3)]. The damage rate equation can be rearranged into the following form in terms of initial and final damage rate.

$$\phi = \frac{1}{1-\omega_0} \ln\left(\frac{\dot{\omega}_{\text{final}}}{\dot{\omega}_{\min}}\right) \tag{5.1}$$

An initial guess value of ϕ is assumed based on prior studies to calibrate the initial damage rate, $\dot{\omega}_0$ using the [Eq. (4.2)] [35,53]. Initial damage, ω_0 is calibrated by setting the worst-case temperature and stress fluctuation to encapsulate the remaining uncertainty in the MCSR data. Material constant, ϕ is determined by employing [Eq. (5.1)] and numerically refined to find the best-fit specimen-specific ϕ constant. The calibrated specimen-specific λ and ϕ are employed later during probabilistic predictions.

Table 5.3 : Fixed material constants for Sinh model of alloy 18Cr-8Ni and 18Cr-12Ni-Mo

Material	Q_c	A^*	σ_s	M^*	σ_t	χ
	$(\text{kJ}\cdot\text{mol}^{-1})$	$(\%\cdot\text{hr}^{-1}\times10^{17})$	(MPa)	$(\text{hr}^{-1}\times10^{17})$	(MPa)	
18Cr-8Ni	414.7	8.50	11.5	9.092	58	3
18Cr-12Ni-Mo	402.9	3.00	11.5	1.507	59	3

5.4.3 Probabilistic Calibration

The probabilistic calibration follows the similar approach explained in Chapter 4. The distribution shape and parameter for the sources of uncertainty are estimated by ASTM standard, CDM-laws, and Anderson-Darling (AD) goodness-of-fit test. The sources of uncertainty with the respective distribution shape and parameter are summarized in Table 5.4.

Table 5.4 : Probability distributions shapes and parameters for sources of uncertainty

Parameter	Distribution Shape	Alloy 18Cr-8Ni	Alloy 18Cr-12Ni-Mo
σ	Normal Gaussian	$\mu = X$ MPa*, $\sigma = X \times (6.4\%/8)$ MPa	$\mu = X$ MPa*, $\sigma = X \times (6.4\%/8)$ MPa
T	Normal Gaussian	$\mu = X\,°C^{*},\ \sigma = 4°C/8$	$\mu = X\,°C^{*},\ \sigma = 4°C/8$
ω_0	Exponential	$\mu = 0.05$	$\mu = 0.05$
λ_0	2-Parameter Weibull	$a = 5.006,\ b = 3.565$	$a = 2.758,\ b = 2.043$
ϕ_0	2-Parameter Weibull	$a = 3.553,\ b = 2.458$	$a = 19.872,\ b = 3.016$

*X is the nominal stress/temperature of interest.

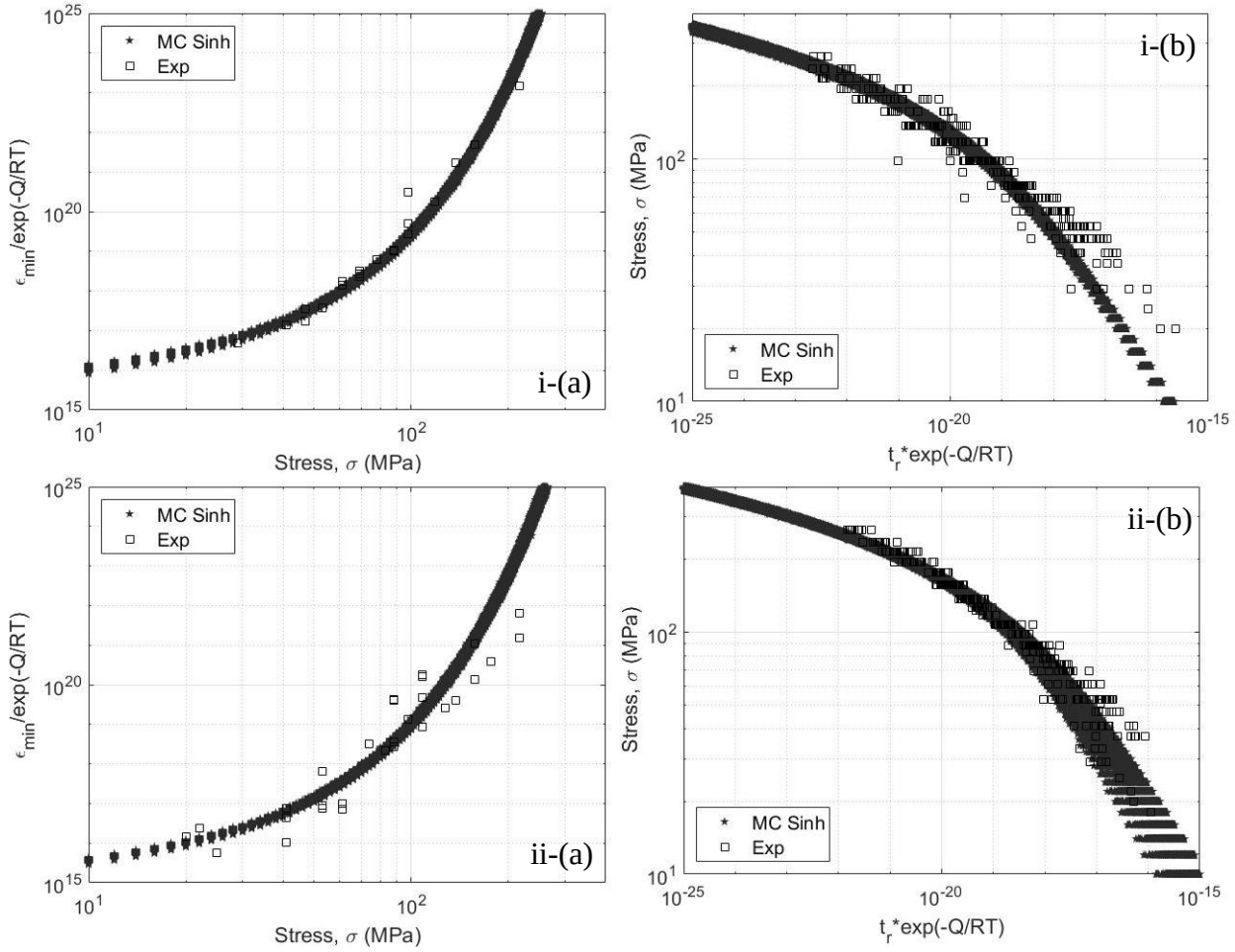

Figure 5.4: "Normalized" (a) MCSR and (b) SR prediction employing the probabilistic Sinh model for (i) alloy 18Cr-8Ni and (ii) alloy 18Cr-12Ni-Mo

5.4.4 Probabilistic Prediction

The probabilistic Sinh prediction for the "normalized" MCSR and SR are accomplished employing the MATLAB subroutine developed in Chapter 4. The predictive capability of the probabilistic Sinh is validated by comparing the "normalized" MCSR and SR prediction with experiment as shown in Figure 5.4. The good-of-fit of the probabilistic prediction is satisfactory. The model prediction resides within the experimental bounds across multiple isostress. The probabilistic prediction tends to show conservative prediction. The predicted MCSR and SR scatter bands exhibit the design point for future modeling of complex components exposed to high stress

and temperature. Based on the prediction, a design decision can be made on the associated safety factor and remaining lifetime of the components. The model does not capture all the experimental uncertainty at lower stress. Several reasons of such behavior are explained in the previous chapter. However, the probabilistic Sinh can generate reasonable prediction across the material databases given the right material properties, fixed constants, and probabilistic parameters.

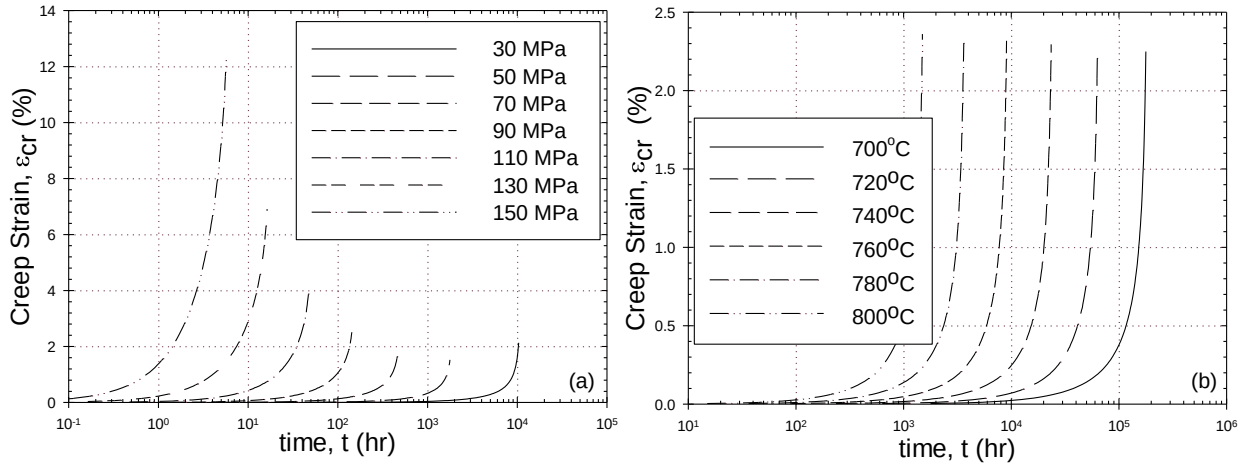

Figure 5.5: Parametric simulation with (a) constant temperature at 750°C and (b) constant loading at 30 MPA for alloy 18Cr-8Ni

5.5.5 Parametric Simulation

In this verification and validation study, an approximation approach is followed to calibrate the material constants (λ, ϕ). In prior studies, these material constants (λ, ϕ) are calibrated directly from the creep deformation curves [35,53]. It requires a new approach for calibration of these material constants when there are no experimental creep deformation curves. For performing the parametric simulation, the Advanced Ultra Super Critical (A-USC) power plants service condition is chosen. Such power plants typically operate between 1300-1400°F (704-760°C) and 4000-5000 psi (27.57-34.47 MPa). In this parametric case study, temperature starting at 700°C and stress starting at 30 MPa is employed. The closed- form Sinh creep strain equation [Eqs. (4.14) and

(4.13)] is employed to produce the creep deformation curves. Note that, the material constant calibrated for 18Cr-8Ni are employed. The parametric simulation result shows expected trend of creep deformation curves. With increasing temperature and stress, a decreasing trend of rupture and an increasing trend of creep ductility is noticed. At high temperature-stress regime, such behavior of the creep deformation curves verified the reliability of the approximation method adopted in absence of full creep deformation curves.

Chapter 6: Conclusion and Future Work

6.1 Conclusion

The objective of this study was to investigate and convert the CDM-based deterministic Sinh model into a probabilistic model by incorporating the uncertainty of creep. The deterministic calibration reveals the inherent uncertainty associated with model constants. The probabilistic calibration determines the distribution shape and parameter of the sources of uncertainty. Monte carlo sampling is employed to generate the individual source and full interaction probabilistic prediction of MCSR, SR, and creep ductility. The assessment led to the following insights.

- The deterministic prediction of MCSR, SR, and creep ductility are accurate, with a mean error between the model and experiment data at 10.433, 0.000, and 8.978%, respectively.
- The individual probabilistic predictions at 320 MPa and 600°C, show that the MCSR, SR, and creep ductility are most influenced by initial damage, stress, and the damage trajectory constant at 97.410, 89.631, and 78.444% of relative effect, respectively. These relative effects change as a function of stress and temperature.
- The full interaction probabilistic predictions of MCSR and SR agree with the experimental data exhibiting a similar scatter band across multiple isotherms. The extrapolation when there is no experimental observation show that the relative scatter bands in MCSR and SR tends to decrease at low-stress matching "normalized" MCSR and SR prediction. The predicted MCSR and SR scatter bands remain consistent for individual isotherms.
- The full interaction creep deformation predictions fit the experimental data across the multiple isostress-isotherms conditions. The qualitative predictions of MCSR,

SR, and creep ductility at 600 and 700°C are satisfactory. At 650°C, prediction at 260 MPa lacks in accurate creep ductility prediction due to 100% underprediction of fixed material constant, A_0 while at 240 MPa, show shorter rupture prediction due to 39% under-prediction of fixed material constant, M^*.

- Overall, the proposed probabilistic model is good for interpolation but lacks in extrapolation ability.

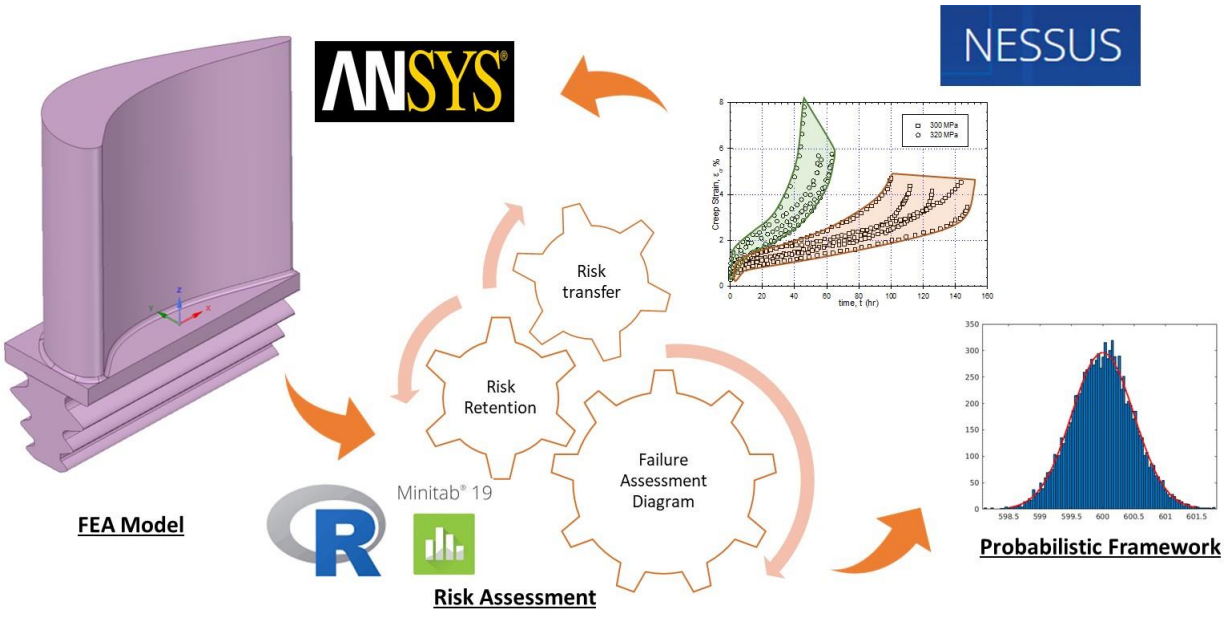

Figure 6.1: Reliability assessment of a turbine blade simulation with probabilistic tools.

6.2 Future Work

The avenues of future work in this field of study are many. The future investigation will introduce the multi-stage Sinh model. The current model lacks in modeling of primary creep stage. Incorporation of time-, strain-, and mixed/work hardening viscous function will enable the model to generate realistic creep deformation curves. The addition of stochasticity into the proposed

probabilistic model will facilitate the application at an industrial setup where the prevailing service condition uncertainty is cruder. The time-dependent pdfs will capture the variation in material constants as a function of time. As Sinh is a phenomenological model, different micro-structural degradation at component level are beyond the scope of the model. Inserting the micro- and meso-scale degradation and material behavior will enhance the accuracy of the probabilistic prediction. The probabilistic tool NESSUS will be employed in conjunction with ANSYS to simulate the FEA 1D, 2D, and 3D model for reliability assessment of critical components e.g. turbine blade as shown in Figure 6.1. There is scope to apply the probabilistic model to Accelerated Creep Testing (ACT) data to extrapolate the creep response of a new candidate alloy across multiple isostress-isotherm [73].

Disclaimer

This material is based upon work supported by the Department of Energy National Energy Technology Laboratory under Award Number(s) DE-FE0027581.

References

[1] Haque, M. S. (2018). *An Adaptive Creep Modeling Approach using Metamodeling*. The University of Texas at El Paso.

[2] Janawitz, J., Masso, J., & Childs, C. (2015). Heavy-duty gas turbine operating and maintenance considerations. *GER: Atlanta, GA, USA*.

[3] Cuzzillo, B. R., & Fulton, L. K. (2014). Failure Analysis Case Studies. Retrieved October 27, 2019.

[4] https://mits.nims.go.jp/index_en.html

[5] Vojdani, A., Farrahi, G. H., Mehmanparast, A., & Wang, B. (2018). Probabilistic assessment of creep-fatigue crack propagation in austenitic stainless steel cracked plates. *Engineering Fracture Mechanics*, *200*(April), 50–63. https://doi.org/10.1016/j.engfracmech.2018.07.022

[6] Mao, H., & Mahadevan, S. (2000). Reliability analysis of creep-fatigue failure. *International Journal of Fatigue*, *22*(9), 789–797. https://doi.org/10.1016/S0142-1123(00)00046-3

[7] Davies, R. B., Hales, R., Harman, J. C., & Holdsworth, S. R. (1999). Statistical Modeling of Creep Rupture Data. *Journal of Engineering Materials and Technology, Transactions of the ASME*, *121*(3), 264–271.

8] Zentuti, N. A., Booker, J. D., Bradford, R. A. W., & Truman, C. E. (2018). Correlations between creep parameters and application to probabilistic damage assessments. *International Journal*

of Pressure Vessels and Piping, *165*(July), 295–305. https://doi.org/10.1016/j.ijpvp.2018.07.004

[9] Betten, J. (2008). *Creep mechanics*. Springer Science & Business Media.

[10] Naumenko, K., & Altenbach, H. (2007). *Modeling of creep for structural analysis*. Springer Science & Business Media.

11] Viswanathan, R. (1989). *Damage mechanisms and life assessment of high temperature components*. ASM international.

[12] Meyers, M. A., & Chawla, K. K. (2008). *Mechanical behavior of materials*. Cambridge university press.

[13] Altenbach, H. (2002). Creep analysis of Thin-Walled structures. *ZAMM-Journal of Applied Mathematics and Mechanics/Zeitschrift für Angewandte Mathematik und Mechanik: Applied Mathematics and Mechanics*, *82*(8), 507-533.

[14] Altenbach, H., Gorash, Y., & Naumenko, K. (2008). Steady-state creep of a pressurized thick cylinder in both the linear and the power law ranges. *Acta Mechanica*, *195*(1-4), 263-274.

[15] Neubauer, B. (1983). Restlife estimation of creep components by means of replica. *Advances in life prediction methods*.

[16] Hayhurst, D. R. (2001). Computational Continuum Damaged Mechanics: Its use in the Prediction of Creep in Structures—Past, Present and Future. In *IUTAM symposium on creep in structures* (pp. 175-188). Springer, Dordrecht.

[17] Rutman, W., Krause, M., & Kremer, K. J. (1966). 'International Community Tests on Long-Term Behavior of 2 1 4 Cr-1 Mo Steel. In *Proc. Joint. Conf. On High-Temperature Properties of Steels* (pp. 232-239).

[18] Garofalo, F., Whitmore, R. W., Domis, W. F., & Vongemmingen, F. (1961). Creep and Creep-Rupture Relationships in an Austenitic Stainless-Steel. *Transactions of the Metallurgical Society of AIME, 221*(2), 310-319.

[19] Penny, R. K., & Weber, M. A. (1992). Robust methods of life assessment during creep. *International Journal of Pressure Vessels and Piping, 50*(1-3), 109-131.

[20] Hayhurst, D. R. (1974). The effects of test variables on scatter in high-temperature tensile creep-rupture data. *International Journal of Mechanical Sciences, 16*(11), 829-841.

[21] Farris, J. P., Lee, J. D., Harlow, D. G., & Delph, T. J. (1990). On the scatter in creep rupture times. *Metallurgical Transactions A, 21*(1), 345-352.

[22] Kim, S. J., Kong, Y. S., Roh, Y. J., & Kim, W. G. (2008). Statistical properties of creep rupture data distribution for STS304 stainless steels. *Materials Science and Engineering: A, 483*, 529-532.

[23] Evans, M. (1994). A statistical analysis of the failure time distribution for ½Cr½Mo¼V steel tubes in the presence of outliers. *International journal of pressure vessels and piping, 60*(2), 193-207.

[24] Booker, M. K., Booker, B. L. P., & Swindeman, R. W. (1982). *Analysis of elevated-temperature tensile and creep properties of normalized and tempered 2 1/4 Cr-1 Mo steel* (No. ORNL/TM-8075). Oak Ridge National Lab., TN (USA).

[25] Calude, C. S. (2013). *Information and randomness: an algorithmic perspective*. Springer Science & Business Media.

[26] Tillé, Y. (2006). *Sampling algorithms* (pp. 31-39). Springer New York.

[27] Kroese, D. P., Taimre, T., & Botev, Z. I. (2013). *Handbook of monte carlo methods* (Vol. 706). John Wiley & Sons.

[28] Zio, E. (2013). System reliability and risk analysis. In *The Monte Carlo simulation method for system reliability and risk analysis* (pp. 7-17). Springer, London.

[29] Haque, M. S., & Stewart, C. M. (2016, July). Modeling the creep deformation, damage, and rupture of Hastelloy X Using MPC omega, theta, and sin-hyperbolic models. In *Pressure Vessels and Piping Conference* (Vol. 50428, p. V06AT06A050). American Society of Mechanical Engineers.

[30] Haque, M. S., & Stewart, C. M. (2016, July). Exploiting Functional Relationships Between MPC Omega, Theta, and Sinh-Hyperbolic Continuum Damage Mechanics Model. In *Pressure Vessels and Piping Conference* (Vol. 50428, p. V06AT06A052). American Society of Mechanical Engineers.

[31] Cano, J. A., & Stewart, C. M. (2019, June). Application of the Wilshire Stress-rupture and Minimum-Creep-Strain-Rate Prediction Models for Alloy P91 in Tube, Plate and Pipe Form. In *Turbo Expo: Power for Land, Sea, and Air* (Vol. 58684, p. V07AT31A007). American Society of Mechanical Engineers.

[32] Perez, J., & Stewart, C. M. (2019, June). Assessment of the Theta Projection Model for Interpolating Creep Deformation. In *Turbo Expo: Power for Land, Sea, and Air* (Vol. 58684, p. V07AT31A002). American Society of Mechanical Engineers.

[33] Appalanaidu, Y., Vyas, Y., & Gupta, S. (2013). Stochastic creep damage growth due to random thermal fluctuations using continuum damage mechanics. *Procedia Engineering*, *55*, 805-811.

[34] Harlow, D. G., & Delph, T. J. (1995). A computational probabilistic model for creep-damaging solids. *Computers & structures*, *54*(1), 161-166.

[35] Hossain, M. A., & Stewart, C. M. (2019, July). Reliability Prediction of 304 Stainless Steel Using Sine-Hyperbolic Creep-Damage Model with Monte Carlo Simulation Method. In *Pressure Vessels and Piping Conference* (Vol. 58974, p. V06AT06A039). American Society of Mechanical Engineers.

[36] Hossain, M. A., Cano, J. A., & Stewart, C. M. (2020). Probabilistic Creep Modeling of 304 Stainless Steel using a Modified Wilshire Creep-Damage Model. *Proceedings of ASME 2020 Pressure Vessel and Piping Conference PVP2020*. American Society of Mechanical Engineers.

[37] Appalanaidu, Y., Roy, A., & Gupta, S. (2014). Stochastic creep damage estimation in pipings with spatial non-gaussian uncertainties using spectral stochastic finite element method. *Procedia Engineering*, *86*, 677-684.

[38] Kim, W. G., Park, J. Y., Hong, S. D., & Kim, S. J. (2011). Probabilistic assessment of creep crack growth rate for Gr. 91 steel. *Nuclear engineering and design*, *241*(9), 3580-3586.

[39] Kim, W. G., Park, J. Y., Hong, S. D., & Kim, S. J. (2011). Probabilistic assessment of creep crack growth rate for Gr. 91 steel. *Nuclear engineering and design*, *241*(9), 3580-3586.

[40] Bhattacharya, B., & Ellingwood, B. (1998). Continuum damage mechanics-based model of stochastic damage growth. *Journal of engineering mechanics*, *124*(9), 1000-1009.

[41] Kim, W. G., Park, J. Y., Kim, S. J., & Jang, J. (2013). Reliability assessment of creep rupture life for Gr. 91 steel. *Materials & Design*, *51*, 1045-1051.

[42] Zhao, J., Li, D. M., Zhang, J. S., Feng, W., & Fang, Y. Y. (2009). Introduction of SCRI model for creep rupture life assessment. *International journal of pressure vessels and piping*, *86*(9), 599-603.

[43] Kim, S. J., Kong, Y. S., Roh, Y. J., & Kim, W. G. (2008). Statistical properties of creep rupture data distribution for STS304 stainless steels. *Materials Science and Engineering: A*, *483*, 529-532.

[44] American Society for Testing and Materials (ASTM). (2011). ASTM E139-11. Standard Test Methods for Conducting Creep, Creep-Rupture, and Stress-Rupture Tests of Metallic Materials.

[45] Krempl, E. (1979). An experimental study of room-temperature rate-sensitivity, creep and relaxation of AISI type 304 stainless steel. *Journal of the Mechanics and Physics of Solids*, *27*(5-6), 363-375.

[46] Manson, S. S., & Haferd, A. M. (1953). A linear time-temperature relation for extrapolation of creep and stress-rupture data.

[47] Larson, F. R. (1952). A time-temperature relationship for rupture and creep stresses. *Trans. ASME*, *74*, 765-775.

[48] Monkman, F. C., & Grant, N. J. (1956). American society of testing materials. *Process*, *56*, 593-620.

[49] Stewart, C. M., & Gordon, A. P. (2010, January). Analytical Method to Determine the Tertiary Creep Damage Constants of the Kachanov-Rabotnov Constitutive Model. In *ASME International Mechanical Engineering Congress and Exposition* (Vol. 44465, pp. 177-184).

[50] Stewart, C. M., & Gordon, A. P. (2012). Strain and damage-based analytical methods to determine the Kachanov–Rabotnov tertiary creep-damage constants. *International Journal of Damage Mechanics*, *21*(8), 1186-1201.

[51] Stewart, C. M. (2013). *A hybrid constitutive model for creep, fatigue, and creep-fatigue damage.* University of Central Florida

[52] Haque, M. S., & Stewart, C. M. (2016). Finite-Element Analysis of Waspaloy Using Sinh Creep-Damage Constitutive Model Under Triaxial Stress State. *Journal of Pressure Vessel Technology*, *138*(3).

[53] Haque, M. S., & Stewart, C. M. (2017). The stress-sensitivity, mesh-dependence, and convergence of continuum damage mechanics models for creep. *Journal of Pressure Vessel Technology*, *139*(4).

[54] Haque, M. S., & Stewart, C. M. (2019). The disparate data problem: The calibration of creep laws across test type and stress, temperature, and time scales. *Theoretical and Applied Fracture Mechanics*, *100*, 251-268.

[55] Miller, A. (1976). An inelastic constitutive model for monotonic, cyclic, and creep deformation: part II—application to type 304 stainless steel. *Journal of Engineering Materials and Technology*, *98(2)*, 106-112

[56] Standard, A. S. T. M. (2004). E8. Standard test method for tension testing of metallic materials. *West Conshohocken (USA): ASTM*.

[57] Dyson, B. F., & McLean, D. (1972). A new method of predicting creep life. *Metal Science Journal*, *6*(1), 220-223.

[58] Middleton, C. J. (1981). Reheat cavity nucleation and nucleation control in bainitic creep-resisting low-alloy steels: roles of manganese sulphide, residual, and sulphur-stabilizing elements. *Metal Science*, *15*(4), 154-167.

[59] Bae, D. H., & Ghosh, A. K. (2002). Cavity formation and early growth in a superplastic Al–Mg alloy. *Acta materialia*, *50*(3), 511-523.

[60] Needham, N. G., & Gladman, T. (1980). Nucleation and growth of creep cavities in a type 347 steel. *Metal science*, *14*(2), 64-72.

[61] Gupta, C., Toda, H., Schlacher, C., Adachi, Y., Mayr, P., Sommitsch, C., ... & Kobayashi, M. (2013). Study of creep cavitation behavior in tempered martensitic steel using synchrotron micro-tomography and serial sectioning techniques. *Materials Science and Engineering: A*, *564*, 525-538.

[62] Kar, J., Dinda, S. K., Roy, G. G., Roy, S. K., & Srirangam, P. (2018). X-ray tomography study on porosity in electron beam welded dissimilar copper–304SS joints. *Vacuum*, *149*, 200-206.

[63] Slotwinski, J. A., Garboczi, E. J., & Hebenstreit, K. M. (2014). Porosity measurements and analysis for metal additive manufacturing process control. *Journal of research of the National Institute of Standards and Technology*, *119*, 494.

[64] Stewart, C. M., & Gordon, A. P. (2012). Constitutive Modeling of Multistage Creep Damage in Isotropic and Transversely Isotropic Alloys with Elastic Damage. *Journal of pressure vessel technology*, *134*(4).

[65] Viswanathan, R. (1989). *Damage mechanisms and life assessment of high temperature components*. ASM international.

[66] Viswanathan, R. (1977). Effect of stress and temperature on the creep and rupture behavior of a 1.25 Pct chromium—0.5 Pct molybdenum steel. *Metallurgical Transactions A*, *8*(6), 877-884.

[67] Lin, G. (1999). ANSYS User Material Subroutine USERMAT. *ANSYS, Canonsburg, PA.*

[68] Oradei-Basile, A., & Radavich, J. F. (1991). A current TTT diagram for wrought alloy 718. *Superalloys*, *718*(625), 325-335.

[69] Lindwall, G., Campbell, C. E., Lass, E. A., Zhang, F., Stoudt, M. R., Allen, A. J., & Levine, L. E. (2019). Simulation of TTT curves for additively manufactured Inconel 625. *Metallurgical and Materials Transactions A*, *50*(1), 457-467.

[70] Hossain, M. A., & Stewart, C. M. (2020). Probabilistic Minimum-Creep-Strain-Rate and Stress-Rupture Prediction for the Long-Term Assessment of IGT Components. In *Proceedings of ASME Turbo Expo 2020: Turbomachinery Technical Conference and Exposition GT 2020.* American Society of Mechanical Engineers.

[71] NIMS Creep Data Sheet from https://smds.nims.go.jp/MSDS/pdf/sheet/C4BJ.pdf

[72] NIMS Creep Data Sheet from https://smds.nims.go.jp/MSDS/pdf/sheet/C6BJ.pdf

[73] Hossain, M. A., & Stewart, C. M. (2020). Calibration of CDM-based Creep Constitutive Model using Accelerated Creep Testing (ACT) Data. *Proceedings of ASME Turbo Expo 2020: Turbomachinery Technical Conference and Exposition GT2020*. American Society of Mechanical Engineers.

Appendix

Table 9.1 : Specimen-specific material constants for Sinh model of alloy 304 SS

Test ID	Stress, σ	ε_{pr}	A_0	M_o	λ	ϕ	$\dot{\varepsilon}_{\min}$	Exp Rupture time, t_r
	MPa	%	$\%\cdot hr^{-1}\times10^{17}$	$hr^{-1}\times10^{17}$			$\%\cdot hr^{-1}$	hr
				600°C				
320_T1	320	0.85	4.12	10.89	3.16	6.26	0.073	46.05
320_T2	320	1.45	2.49	8.85	1.59	4.08	0.044	56.64
320_T3	320	0.76	2.42	9.14	3.04	5.90	0.043	54.87
320_T4	320	1.20	2.33	7.91	1.85	4.98	0.041	63.36
320_T5	320	0.82	1.68	7.93	2.46	3.01	0.029	63.23
300_T1	300	0.80	3.75	12.37	2.09	7.04	0.025	100.00
300_T2	300	0.82	2.11	11.05	2.72	4.91	0.014	111.86
300_T3	300	0.73	1.96	9.85	3.39	7.24	0.013	125.48
300_T4	300	0.95	2.20	8.61	1.47	3.31	0.015	143.52
300_T5	300	0.63	1.65	8.39	2.25	5.95	0.011	147.43
				650°C				
260_T1	260	0.45	8.05	12.28	2.53	2.98	0.046	26.88
260_T2	260	1.05	8.10	10.21	2.05	3.99	0.017	32.31
260_T3	260	0.83	5.44	10.10	2.79	3.54	0.022	32.67
260_T4	260	0.70	6.89	10.27	3.25	5.85	0.020	32.14
260_T5	260	1.00	4.66	7.83	2.12	3.65	0.017	42.12
240_T1	240	0.70	5.14	6.38	2.57	4.37	0.187	127.61
240_T2	240	0.55	1.98	6.02	2.37	2.49	0.188	135.14
240_T3	240	0.50	2.51	5.57	2.03	3.44	0.126	146.18
240_T4	240	0.70	2.32	5.77	2.25	4.96	0.160	141.10
240_T5	240	0.65	1.96	4.98	2.96	4.05	0.108	163.52
				700°C				
180_T1	180	0.90	6.61	9.03	2.21	4.70	0.056	82.73
180_T2	180	1.55	3.25	8.67	2.78	3.15	0.027	86.14
180_T3	180	0.43	3.52	8.35	3.55	3.51	0.030	89.48

180_T4	180	0.65	3.11	8.31	3.80	3.74	0.026	89.83
180_T5	180	0.60	2.42	8.02	3.05	2.75	0.020	93.12
160_T1	160	1.45	2.67	10.52	4.55	4.22	0.008	176.84
160_T2	160	0.42	2.43	11.86	3.84	3.96	0.007	156.95
160_T3	160	0.41	2.26	11.24	4.39	4.05	0.007	165.63
160_T4	160	0.56	2.14	10.09	4.09	3.89	0.007	184.51
160_T5	160	0.45	1.90	9.47	5.02	4.34	0.006	196.41

Vita

Md Abir Hossain was born in Bangladesh, in 1991. His early schooling was completed in Faujdarhat Cadet College, a feeder institution of Bangladesh Armed Force. He received his bachelor's degree from Bangladesh University of Engineering and Technology (BUET) in 2016 from the Department of Naval Architecture and Marine Engineering (NAME). He became a Lecturer in the Department of Naval Architecture and Marine Engineering (NAME) of Military Institute of Science and Technology (MIST) from July 2016 to December 2017. In pursuit of higher studies, Mr. Hossain got admission in the PhD program of The University of Texas at El Paso in the Fall 2018. In his time at UTEP, Mr. Hossain remains a Doctoral Research Assistant in the Material at Extreme Research Group (MERG). His research focuses on the probabilistic creep-damage modeling, uncertainty quantification, life-time prediction of critical component exposed to high temperature and loading. He is the author of several scholarly articles as well as paper presentation at International conferences. He served as a reviewer for ASME conference and a student member of ASME since 2018. He has been awarded Travel grants from the Graduate School in 2019 and 2020. He participated in several ASME conferences and DOE annual review meeting.

Contact Information: mhossain9@miners.utep.edu